Quaternary Science Reviews 212 (2019) 149–163

Contents lists available at ScienceDirect

Quaternary Science Reviews

journal homepage: www.elsevier.com/locate/quascirev

Geochemical evidence for provenance diversity of loess in southern China and its implications for glacial aridification of the northern subtropical region

Long Han [a, b], Qingzhen Hao [a, b, c, *], Yansong Qiao [d], Luo Wang [a, b, e], Shuzhen Peng [f], Nan Li [g], Xinbo Gao [a, e], Yu Fu [a, b], Bin Xu [a, b, e], Zhaoyan Gu [a, b, e]

[a] Key Laboratory of Cenozoic Geology and Environment, Institute of Geology and Geophysics, Chinese Academy of Sciences, Beijing, 100029, China
[b] University of Chinese Academy of Sciences, Beijing, 100049, China
[c] Center for Excellence in Life and Paleoenvironment, Chinese Academy of Sciences, Beijing, 100044, China
[d] Institute of Geomechanics, Chinese Academy of Geological Sciences, Beijing, 100081, China
[e] Institutions of Earth Science, Chinese Academy of Sciences, Beijing, 100029, China
[f] Key Laboratory of Tourism and Resources Environment in Universities of Shandong, Taishan University, Taian, 271021, China
[g] School of Earth and Space Sciences, Peking University, Beijing, 100871, China

ARTICLE INFO

Article history:
Received 8 January 2019
Received in revised form
28 March 2019
Accepted 1 April 2019

Keywords:
Xiashu loess
Provenance
Geochemistry
Alluvial plain
Aridification
Last glacial period
Huai river
Yangtze river

ABSTRACT

The thick '*Xiashu* loess' in southern China is distributed not only in the Yangtze River valley, but also and most extensively in the region between the Qinling Mountains and the lower reaches of the Yangtze River. However, there are few studies of the provenance and climatic implications of the *Xiashu* loess in this latter region. Here we present the results of a provenance study of Last Glacial loess samples from twenty-two typical *Xiashu* loess sections, using the major and trace element composition as a provenance indicator. Seventeen of the sites are located to the north of the Yangtze River and our primary aim was to determine the provenance of the *Xiashu* loess within this region. Our results indicate that the alluvial plain located mainly in the present drainage area of the Huai River was the primary dust source for the *Xiashu* loess in this region. The occurrence of multiple local dust sources within this alluvial plain, suggested by their geochemical heterogeneity, indicates that the alluvial plain experienced intensified aridity which caused it to become a dust source for local loess deposits in northern subtropical China during the Last Glacial. Our study provides strong evidence to challenge the long-held view that the occurrence of *Xiashu* loess resulted from the southward incursion of the CLP loess deposits sourced from deserts of the Asian interior, and it confirms the substantial role of aridification of the present humid northern subtropical region for dust emission to the climate system during the Last Glacial.

1. Introduction

Knowledge of the provenance of loess sediments provides crucial information about climate changes within the dust source region (Guo et al., 2002; Sun et al., 2010), and about dust transport by atmospheric circulation (Muhs and Bettis, 2000; Smith et al., 2003; Aleinikoff et al., 2008). In addition, tracing loess provenance can provide a basis for the climatic interpretation of proxy records, because dust from different source areas may have different physicochemical properties (Chen et al., 2007; Yang et al., 2008; Li et al., 2009a). As loess deposits are the most widely distributed terrestrial dust archive, knowledge of their provenance and its temporal variations can also provide important constraints for the numerical modelling of dust transport.

The widespread loess-paleosol sequences in southern China, which are termed '*Xiashu* loess' (Li et al., 1935), provide long terrestrial records of paleoenvironmental change in the northern subtropical region. The largest area of loess distribution is in the region to the east of the Tongbai and Dabie Mountains, between the Yangtze River and the Qinling Mountains (Fig. 1a and c); however, only the *Xiashu* loess in the Yangtze River valley has been

* Corresponding author. Key Laboratory of Cenozoic Geology and Environment, Institute of Geology and Geophysics, Chinese Academy of Sciences, Beijing, 100029, China.
E-mail address: haoqz@mail.iggcas.ac.cn (Q. Hao).

https://doi.org/10.1016/j.quascirev.2019.04.002
0277-3791/

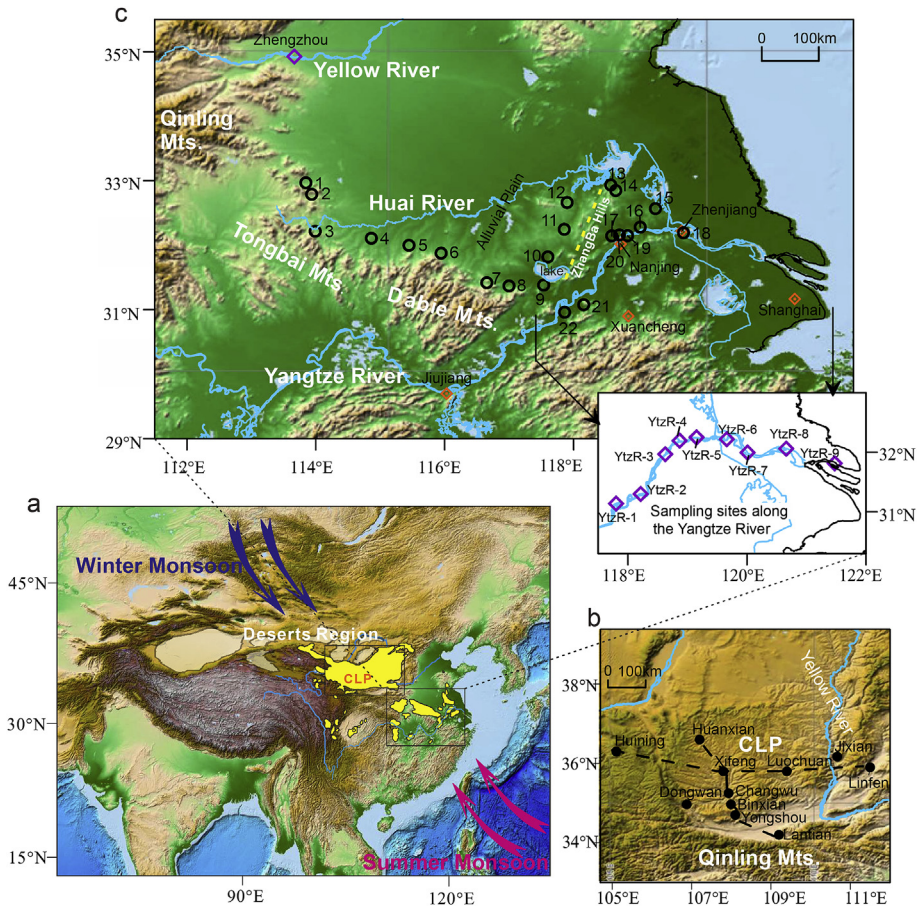

Fig. 1. Study area and the location of the sites mentioned in the text. (a) Chinese Loess Plateau (CLP) and loess distribution in southern China (the loess area is modified from Liu (1985)); (b) CLP sites (black solid circles) studied or mentioned in the text; (c) the *Xiashu* loess sections in southern China (black open circles), and sampling locations of sediments from the Yangtze River and the Yellow River (purple open diamonds). The base maps are from https://maps.ngdc.noaa.gov/viewers/wcs-client. In Fig. 1c, the Yellow dashed line highlights 'Zhangba Hills' with altitude less than 400 m. The east-west trending Qingling Mts. and the Huai River are the traditional boundary between temperate northern China and subtropical southern China. Section names: 1—Yifeng, 2—Queshan, 3—Youhe, 4—Zhaihe, 5—Shangcheng, 6—Sungang, 7—Lu'an, 8—Nangang, 9—Muji, 10—Feidong, 11—Dingyuan, 12—Sanhe, 13—Xuyi, 14—Jiupu, 15—Yangzhou, 16—Yizheng, 17—Laoshan, 18—Dagang, 19—Yanziji, 20—Yangjiang, 21—Suncun, 22—Tongling. (For interpretation of the references to color in this figure legend, the reader is referred to the Web version of this article.)

investigated intensively (Qiao et al., 2003, 2011; Hao et al., 2010; Liu et al., 2014; Li et al., 2017a,b; Wang et al., 2017). Thick *Xiashu* loess deposits in these northern regions are distributed on river terraces, in the lee of the gentle slopes of the low hills, and in other typical geomorphological settings such as tableland. The thick loess-paleosol sequences in these regions (Xu, 1991; Zhang and Song, 2013; Guan et al., 2016; Li et al., 2017b) have a similar thickness and deposition age to the classical Xuancheng and Jiujiang sections (Qiao et al., 2003, 2011). These loess-paleosol sequences comprise valuable paleoclimatic archives in the northern subtropical region of the East Asian monsoon regime; more specifically, they can potentially improve our understanding of the spatiotemporal variability of the East Asian monsoon, and provide crucial information on climatic evolution within the dust source regions.

Significant progress has been made in the study of the provenance of the *Xiashu* loess distributed in the Yangtze River valley. The prevailing view is that these southern loess deposits are mainly derived from the Asian interior deserts, as is the case for the well-documented loess of the Chinese Loess Plateau (CLP) (Liu, 1985; Yang, 1991; Li et al., 2001), and this view was popular until the early 21st century. An alternative view is that the fine-grained fluvial deposits in the Yangtze River valley and/or adjacent lake beds (e.g. Yang, 1986; Qiao et al., 2003), or the continental shelf exposed during glacial periods (Zhao and Li, 1990), made an important contribution. This interpretation was supported by evidence of the paleogeographical evolution of the Yangtze River during the Last Glacial (Yang, 1986; Liu et al., 1997). Although it was long ignored, recent evidence from analyses of major and trace elements (Hao et al., 2010), Nd isotopes (Qiao et al., 2011; Hong et al., 2013), zircon U-Pb ages (Liu et al., 2014; Wang et al., 2017) and uranium comminution ages (Li et al., 2017a), has revealed distinct geochemical differences between the *Xiashu* loess distributed in the Yangtze River valley and the loess deposits of the CLP. Most of these studies suggest that the fluvial deposits of the Yangtze River make the major contribution to these loess deposits, which is consistent with the relationship between loess and rivers, as summarized for example by Smalley et al. (2009).

However, due to our limited knowledge of the provenance of loess to the north of the Yangtze River, the largest area of *Xiashu* loess distribution (Fig. 1c), the environmental implications of the occurrence of the widespread loess deposits in southern China remain unclear. It seems unlikely that the loess deposits between the Qinling Mts. and the Yangtze River are mainly sourced from the Yangtze River valley. Overall, it is unknown whether these loess deposits came from the deserts in the Asian interior or from local sources. The former case would suggest that these loess deposits reflect intensified arid conditions in the northwestern deserts and a strengthened East Asian winter monsoon, while the latter case

would suggest that they reflect aridification of the adjacent alluvial plain. Although we have speculated previously that these loess deposits are sourced from the local alluvial plain (Hao et al., 2010), geochemical evidence is needed to confirm this.

Here we report the results of analyses of grain-size components and the major and trace element composition of samples of Last Glacial loess from 22 *Xiashu* loess sections. Seventeen of these sections are distributed in the region to the north of the Yangtze River, and five are from the Yangtze River valley. We compared their geochemical composition with those of three important dust potential source areas: the Yangtze River valley, the Yellow River valley, and the northwestern deserts in the Asian interior. The average geochemical composition of the northwestern deserts was inferred from the downwind eolian deposits from the CLP, and the ratios of relatively immobile elements of the <20 μm fraction were employed for provenance tracing. Our main aims were: 1) to trace the provenance of loess in the region between the Qingling Mts. and the Yangtze River (hereinafter termed 'northern *Xiashu* loess'), 2) to determine the contribution of Yangtze/Yellow River sediments to *Xiashu* loess, and 3) to explore the climatic context within the dust source areas.

2. Materials and methods

2.1. Xiashu loess samples

In northern subtropical China, the *Xiashu* loess is widely distributed in the alluvial plain of the present Huai River drainage (namely the Huai River Plain or Huang-Huai Plain) and in the lower reaches of the Yangtze River (Fig. 1). The Zhangba Hills, close to the northern bank of the Yangtze River (Fig. 1c), comprise the watershed between the Yangtze River and the Huai River. To better understand the provenance of loess in these regions, we obtained samples from 22 sections, with the focus on the northern *Xiashu* loess (i.e. the loess to the north of the Yangtze River). Among the 22 sections, sections 1–17 are located to the north of the Yangtze River; more specifically, sections 1–8 are distributed along the piedmont of the Tongbai and Dabie Mts.; sections 9–15 and 17 are from the hilly region (mainly the Zhangba Hills) in the Huai drainage area; section 16, which is located on the river terrace of a tributary of the Yangtze River, is classified as northern *Xiashu* loess, because it is located in the area of low hills to the north of the Yangtze River; and sections 18–22 are in the valley of, or to the south of, the Yangtze River. These sections are distributed in the humid region with mean annual precipitation ranging from approximately 950 to 1100 mm.

The top of the *Xiashu* deposits is the dark brownish Holocene soil, beneath which we obtained loess samples of Last Glacial age. Previous stratigraphic correlation and optically stimulated luminescence data show that the first loess layer in southern China typically corresponds to Marine Isotope Stages (MIS) 2–4 (Xia and Wang, 1999; Hong et al., 2009; Lai et al., 2010; Guan et al., 2016; Yi et al., 2018). Among the 22 sites studied, five samples were typically obtained from each loess section, except for two thin loess sections in which 3–4 samples were taken. Most of the loess sections are typical loess-paleosol sequences, except for the Dianyuan and Sanhe sections (sections 11 and 12) (Fig. 1). In the Dingyuan section (section 11), there is a layer containing 10-cm-thick laminations in between L1 and S0, and L1 contains a minor amount of rock fragments with diameters <2 mm; and in the Sanhe section (section 12), lateral changes in lithology can be observed in the exposed outcrops, and some locations contain coarse debris. For these two sections, secondary loess was carefully avoided during sampling. In total, 107 samples of Last Glacial (L1) loess were obtained from the 22 sections for provenance analyses.

2.2. Loess samples from the Chinese Loess Plateau

The deserts in the Asian interior are a potential dust source for the *Xiashu* loess. In the present study, the eolian deposits of the CLP are used as a reference for the average geochemical composition of the dust from the deserts. Sixteen samples from the CLP were used for comparison: five samples of Pleistocene loess from the Xifeng section (Guo et al., 2000), and one from the late Pleistocene loess unconformably overlying the late Neogene Dongwan sequence in the western CLP (Hao and Guo, 2004); five samples are from the upper part (4.7–2.6 Ma) of the Xifeng Red Earth (Guo et al., 2001); and five samples (3.9–6.8 Ma) are from the Dongwan loess section (Hao and Guo, 2004). The geochemical composition of the <20 μm fraction of the CLP samples (except for the late Neogene deposits from Dongwan) was published in Hao et al. (2010).

In addition, we analyzed the major element abundances of bulk samples from two transects across the CLP, one in a northwest-southeast (NW-SE) direction (Hao et al., 2010) and the other in a west-east (W-E) direction (Fig. 1b), in order to characterize spatial changes in geochemistry of the CLP loess. These samples include both loess of the Last Glacial Maximum and paleosol of the Last Interglacial climatic optimum, from nine sections.

2.3. River sediment samples

Fluvial sediments of the Yangtze River and the Yellow River were also sampled for comparison with the *Xiashu* loess. They are the two largest rivers in China and the sediments exposed in their valleys during glacials are two important potential dust sources. To evaluate the spatial heterogeneity of the major and trace element composition of the fluvial sediments, nine sites at ~50-km intervals along the Yangtze River valley, from Tongling (close to section 22) to the river estuary at Shanghai (Fig. 1c), were sampled. At each site, six samples were taken along the direction normal to the river channel, among which one sample consisted of modern sediments exposed at the river bank during the season of low water level; and the other five samples were taken at distances of 50 m, 150 m, 250 m, 350 m and 450 m away from the river channel. All of the samples were taken at the depth of 30 cm below the surface to avoid contamination by human activity. For the sediment samples from the Yellow River valley, five samples were taken at one site to the west of Zhengzhou city. We evaluated the spatial changes in the composition of the Yellow River sediments via comparison with our previously reported results for sediments at the site downstream (Peng et al., 2016).

At site 5 of the Yangtze River sediments (YtzR-5 in Fig. 1c), the geochemical composition of all the samples was analyzed to reveal any lateral changes in the river sediments. For the other eight sites, the five samples off the channel, except for the modern river bank sediment sample, were combined. This produced two group of samples at each site: one is closest to the river channel and the other one is a mixed sample which represent the floodplain sediments.

2.4. Grain-size analysis

The grain-size distribution of the bulk samples was determined using a Malvern Mastersizer 2000 laser particle-size analyzer, which has a measurement range of 0.02–2,000 μm with a precision of ±1%. Sample pretreatment followed the methods of Hao et al. (2012): removal of organic matter and carbonates with sequential treatment with 10% H_2O_2 and 10% HCl, followed by dispersal with 0.05 N $(NaPO_3)_6$ solution.

2.5. Grain-size separation

The <20 μm fraction has been used to determine dust

provenance (e.g. Sun, 2002; Muhs et al., 2007; Hao et al., 2010). According to Tsoar and Pye (1987), dust particles finer than 20 μm are transported mainly in long-term suspension across a large height range and may be widely dispersed under moderate dust storm conditions. If the deserts of the Asian interior are an important dust source for the deposits of southern China, their equivalent fraction should have a similar geochemical composition. Selection of the relatively uniform <20 μm fraction also reduces the effects of grain size on sedimentary geochemistry and mineralogy.

The bulk samples were pretreated with 10% H_2O_2 and 1 mol/L acetic acid to remove organic matter and carbonate, respectively. They were then rinsed and dispersed by adding 10 ml of 0.05 mol/L $(NaPO_3)_6$ and then ultrasonicated prior to wet sieving using a 62.5 μm mesh screen. The <20 μm fraction was pipetted from suspension based on Stokes' Law.

2.6. Major and trace element analysis

Major element abundances were measured by X-ray fluorescence spectrometry (XRF) using a Panalytical spectrometer at the Institute of Geology and Geophysics, Chinese Academy of Sciences. Fusion glasses were prepared by mixing 0.7 g of powder sample with 7 g of dilithium tetraborate ($Li_2B_4O_7$) and four drops of 1.5% LiBr, followed by heating to 1100 °C in a furnace and then cooling to form a glass disc for XRF analysis. Analytical uncertainties are ±2% for all major elements except for P_2O_5 and MnO (up to ±10%). Weight- loss on ignition (LOI) was determined by weighing before and after heating to 950 °C for 1 h.

Trace elements including REE were determined using an HR-ICP-MS at the Beijing Research Institute of Uranium Geology, Chinese Ministry for Nuclear Industries. 40 mg powder samples were dissolved in a sealed Teflon beaker with 1 ml HF and 0.3 ml (1:1) HNO_3, shaken for 15 min with an ultrasonic device and then heated on a hotplate at ~120 °C for 24 h. After evaporation to dryness, the samples were redissolved in 1 ml HF, 0.3 ml (1:1) HNO_3 and 0.5 ml $HClO_4$ and then heated to 120 °C for 7 days in order to further break down silicates. 2 ml (1:1) HNO_3 was then added again and dried twince until no remaining residue was detectable. Dissolved samples were then diluted to a volume of 49 ml with 1 ml 1% HNO_3, and 500 ppb indium was added as an internal standard for the final measurement. The analytical uncertainties are less than 5% for most of the trace elements.

3. Results

3.1. Grain-size distributions

The grain-size frequency distributions of the top samples from the 22 sections are presented in Fig. 2. All of the studied loess samples have grain-size distributions typical of loess, except for those from sections 11 and 12. The samples from each section have a rather uniform grain-size distribution. For the 20 representative loess sections, the grain size varies from 0.1 to 100 μm and the frequency distributions are predominantly bimodal, with the primary peak (the modal size) varying from roughly 16–32 μm and with the secondary peak at <1 μm. The sole exception is the sample from the bottom of L1 in section 5 which has a very minor third component with a sand-size mode; however, the content of the >63 μm fraction is only 1.9%. The mean contents of the clay (<2 μm), silt (2–63 μm) and sand (>63 μm) fractions are 13.60% (9.65–18.76%), 85.33% (81.11–89.94%) and 1.07% (0–4.34%), respectively. The <20 μm fraction in all of these samples are 67.00% on average (54.56–79.07%). Although these values are typical of eolian dust deposits, the texture is finer than those of the Last Glacial loess samples from the CLP (Hao et al., 2012).

For the two secondary loess sections (sections 11 and 12), the samples have a third sand-sized component with a modal size varying from 240 to 417 μm; however, the other two modes are exactly the same as in the other 20 representative loess sections. The mean contents of the clay (<2 μm), silt (2–63 μm) and sand (>63 μm) fractions are 13.24% (11.33–14.12%), 75.90% (72.52–84.24%) and 10.86% (3.06–14.23%), respectively. It is clear that eolian dust dominates the grain-size distributions of the studied samples.

3.2. Major element geochemistry

The major element composition of the <20 μm fraction of the *Xiashu* loess samples is relatively uniform for each site, although there is a larger range of variation of the mean composition between the 22 sites (Table S1). The mean percentages of SiO_2 and Al_2O_3 of the sections range from 68.03 ± 0.51% to 84.76 ± 0.81%, and from 8.07 ± 0.58% to 17.45 ± 0.59%, respectively; and those of Fe_2O_3 and TiO_2 range from 2.33 ± 0.28% to 6.82 ± 0.61% and from 1.01 ± 0.02% to 1.43 ± 0.15%, respectively. Compared with the CLP samples (Table S2), the <20 μm fraction of the *Xiashu* loess is characterized by higher percentages of SiO_2 and TiO_2, and lower percentages of Al_2O_3, Fe_2O_3, CaO, MgO and K_2O.

However, the major element compositions of the <20 μm fraction of the Yangtze River and the Yellow River samples are different (Table S2). The major element composition of the Yangtze River samples is relatively uniform, although the nine sites in the river valley span a distance of 450 km. The mean percentages of SiO_2 and Al_2O_3 range from 62.06 ± 0.86% to 66.47 ± 1.05% and from 17.06 ± 0.42% to 19.39 ± 0.81%, respectively; and those of Fe_2O_3 and TiO_2 range from 7.17 ± 0.33% to 8.63 ± 0.34%, and from 1.20 ± 0.08% to 1.38 ± 0.07%, respectively. The deviations of the element percentages between samples at each site are mostly less than 3%, which suggests that there is no significant lateral variation in sediment composition. This overall uniform composition of

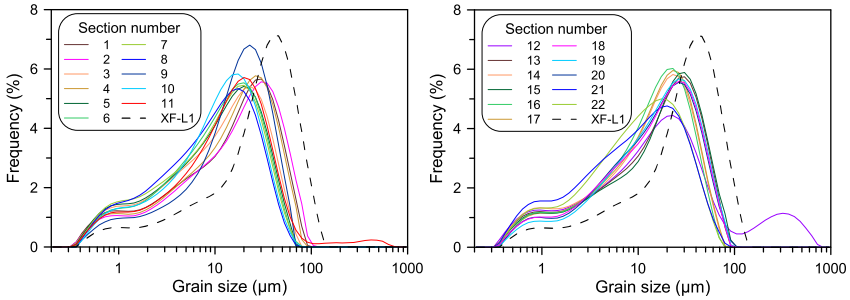

Fig. 2. Grain-size frequency distributions of samples from the 22 *Xiashu* loess sections. The samples are from the top of L1, and the grain-size frequency distribution of L1 of the classical Xifeng section on the Chinese Loess Plateau is shown for comparison (Hao et al., 2012). Section numbers are the same as Fig. 1.

samples along the river may be because there is no large tributary in the lower reaches of the Yangtze River and because sediment sorting does not produce significant variations in geochemical composition. This observation leads us to conclude that a single site in the lower reaches of this type of major river valley may reliably reflect the overall geochemical composition of the fluvial sediments. For the <20 μm fraction of the Yellow River sediments, the percentages of SiO_2 and Al_2O_3 are 67.80% and 15.87%, respectively; and those of Fe_2O_3 and TiO_2 are 6.29% and 0.90%, respectively. These values are similar to those of the sediments in the lower reaches of the Yellow River (36°10′N, 116°20′E) (see Table 2 in Peng et al. (2016)). Compared with the Yellow River, the Yangtze River sediments have higher percentages of Al_2O_3, Fe_2O_3, K_2O and TiO_2, and lower percentages of SiO_2, CaO and Na_2O; in addition, there is no systematic difference in the MgO concentration between the sediments of the two rivers.

The degree of chemical weathering strength can be determined using an Al_2O_3-(CaO*+Na_2O)-K_2O (A-CN-K) triangular diagram and the CIA index (Nesbitt and Young, 1984; Fedo et al., 1995). The A-CN-K plot (Fig. 3) shows that the distribution of the *Xiashu* loess samples lies subparallel to the weathering trend of the A-CN axis, indicating that they are at an early stage of chemical weathering, characterized by the removal of Na and Ca (via plagioclase weathering). By contrast, the content of K hosted by K-feldspars remains unchanged. The chemical index of alteration (CIA) is calculated as follows: $CIA = [Al_2O_3/(Al_2O_3+Na_2O + K_2O + CaO^*)] \times 100$ (molar proportions, and CaO* represents the Ca in silicate minerals). For the *Xiashu* loess samples the CIA ranges from 64.48 ± 1.46 to 75.14 ± 0.71 (Fig. 3), which indicates a moderate weathering strength (CIA = 60–80) (Fedo et al., 1995).

The sediments of the Yellow River (CIA = 64.84) exhibit a lower degree of weathering than those of the Yangtze River (CIA ranges from 70.43 ± 0.49 to 72.44 ± 0.39). All the samples from the 22 *Xiashu* loess sections have CIA values higher than those of the Yellow River sediments, while 16 of them have CIA values lower than the lowest CIA value (70.43) of the Yangtze River sediments.

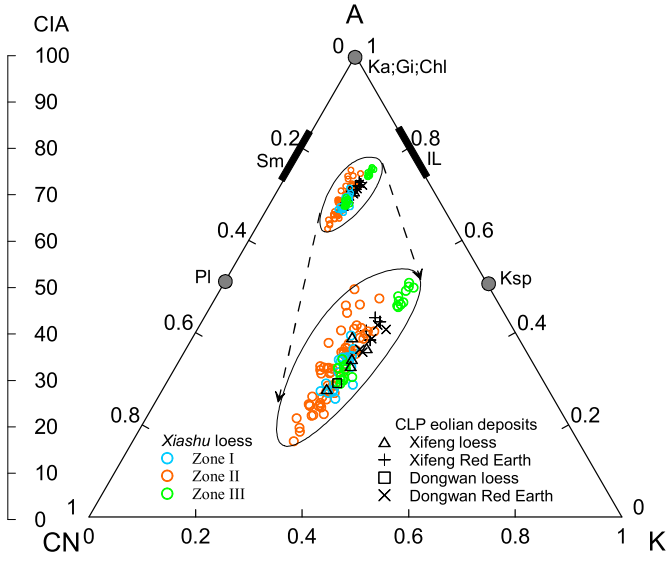

Fig. 3. Geochemical composition of the *Xiashu* loess and the eolian deposits of the CLP plotted as molar proportions on an Al_2O_3-(CaO*+Na_2O)-K_2O (A-CN-K) triangular diagram, together with their CIA values. The molar proportions of the minerals are cited from Fedo et al. (1995). The *Xiashu* loess samples are shown by three different colored symbols according to three zones defined by spatial changes in SiO_2/Al_2O_3 and TiO_2/Al_2O_3 ratios of the *Xiashu* loess shown in Fig. 5. Abbreviations: Sm, smectite; IL, illite; Ksp, potassium feldspar; Pl, plagioclase; Ka, kaolinite; Gi, gibbsite; Chl, chlorite.

The element ratios of TiO_2/Al_2O_3, SiO_2/Al_2O_3 and K_2O/Al_2O_3 are useful for reflecting the mineralogy and geochemistry of dust sources (Sheldon and Tabor, 2009; Hao et al., 2010; Peng et al., 2016). The three ratios exhibit relatively minor changes in the samples at each *Xiashu* loess site, whereas there are substantial changes between the sites (Fig. 4). The mean values of TiO_2/Al_2O_3 and SiO_2/Al_2O_3 for the 22 sections range from 0.07 to 0.18 and from 6.48 to 17.91, respectively; the K_2O/Al_2O_3 ratio is less variable and ranges from 0.17 to 0.22. The variation of these element ratios of *Xiashu* samples within three zones, defined by spatial changes in the values of TiO_2/Al_2O_3 and SiO_2/Al_2O_3 (Fig. 5), are discussed below, with reference to Fig. 5. Compared with the eolian deposits of the CLP, the <20 μm fraction of the 22 *Xiashu* loess sections has distinctly high TiO_2/Al_2O_3 and SiO_2/Al_2O_3 ratios, and a large range of variation of K_2O/Al_2O_3 ratios, with partly overlapping values.

For the <20 μm fraction of the river sediments, the values of TiO_2/Al_2O_3, SiO_2/Al_2O_3 and K_2O/Al_2O_3 for the Yellow River sediments are 0.07, 7.25 and 0.20, respectively; and the mean values of these ratios range from 0.08 to 0.10, from 5.43 to 6.61 and from 0.19 to 0.20 for the Yangtze River sediments, respectively. Compared with the Yellow River sediments studied herein and elsewhere (Peng et al., 2016), the Yangtze River sediments have high TiO_2/Al_2O_3 and low SiO_2/Al_2O_3 values. Overall, the river sediments have a much more restricted range of the three ratios than the *Xiashu* loess samples (Fig. 4).

Spatial changes in the geochemical composition of the *Xiashu* loess are highlighted by a map of the average values of the element ratios of the <20 μm fraction for each loess section (Fig. 5). Three compositional zones can be defined based on the magnitude of TiO_2/Al_2O_3 and SiO_2/Al_2O_3 values; however, spatial changes in K_2O/Al_2O_3 are much less evident. The first zone (Zone I, sections 1–4) is located in the upper reaches of the Huai River, and the values of TiO_2/Al_2O_3 and SiO_2/Al_2O_3 are less than 0.10 and 9.00, respectively. The second subzone (Zone II, sections 5–17) is located between the Huai River and the Yangtze River, and the values of TiO_2/Al_2O_3 and SiO_2/Al_2O_3 range from 0.10 to 0.18 and from 9.00 to 17.83 respectively. The third zone (Zone III, sections 18–22) is located within or south of the Yangtze River valley, where the values are again relatively low. In Zone III, the three eastern sites (sections 18–20) have values of TiO_2/Al_2O_3 and SiO_2/Al_2O_3 of 0.08 and 7.03–7.17; while the two western sites (sections 21 and 22) have values of 0.10 and 0.11, and 8.42 and 9.50, respectively.

In contrast to the significant spatial changes in TiO_2/Al_2O_3 and SiO_2/Al_2O_3 ratios of the *Xiashu* loess, the <20 μm fraction of the Yangtze River sediments has uniform values (the blue solid circles in Fig. 5). Along the river, the values of TiO_2/Al_2O_3, SiO_2/Al_2O_3 and K_2O/Al_2O_3 vary from 0.08 to 0.10, from 5.43 to 6.61 and from 0.19 to 0.20, respectively, and there is no obvious spatial trend.

3.3. Trace element (REE) geochemistry

The mean trace element concentrations (including REE) of the <20 μm fraction of the *Xiashu* loess and of the PSA samples are presented in Tables S3–S6, and the REE parameters and trace element ratios are illustrated in Figs. 6 and 7. As is the case for the major elements, the concentrations of trace elements and REE are rather uniform for the different samples at each loess section, while there is a large degree of variability between sites. REE distributions are conventionally normalized to chondrite values. The europium (Eu) anomaly can be quantified as $Eu/Eu^* = Eu_N/(Sm_N \times Gd_N)^{0.5}$ (where the subscript N denotes chondrite-normalized data). LREE/HREE reflects the fractionation between LREE (light REE group) and HREE (heavy REE group). La_N/Sm_N and Gd_N/Yb_N are indicators of LREE and HREE differentiation, respectively. The chondrite-

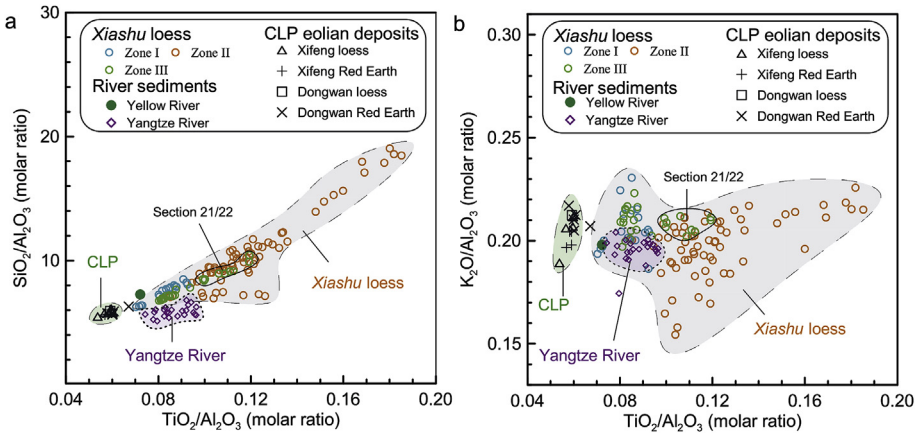

Fig. 4. Plots of (a) SiO_2/Al_2O_3 vs. TiO_2/Al_2O_3 and (b) K_2O/Al_2O_3 vs. TiO_2/Al_2O_3 for the <20 μm fraction of the *Xiashu* loess, the CLP eolian deposits and the river sediments. The *Xiashu* loess samples are shown by three different colored symbols according to three zones defined by spatial changes in SiO_2/Al_2O_3 and TiO_2/Al_2O_3 ratios of the *Xiashu* loess shown in Fig. 5.

normalized REE distribution for the <20 μm fraction of the 107 *Xiashu* loess samples from the 22 sections shows enriched LREE, negative Eu anomalies, and depleted HREE (Fig. 6). This pattern is demonstrated by LREE/HREE varying from 9.56 to 14.16. The values of La_N/Sm_N (4.06–5.12) and Gd_N/Yb_N (1.25–1.53) define steep LREE distributions and relatively flat HREE distributions, respectively. Eu/Eu* ranges from 0.59 to 0.75 and reflects the Eu depletion of the *Xiashu* loess. Thus, the *Xiashu* loess samples have REE distributions typical of upper crustal compositions (UCC).

Compared with the <20 μm fraction of the CLP eolian deposits, the subsamples of the *Xiashu* loess have overall higher LREE/HREE and La_N/Sm_N values (Fig. 6). The Gd_N/Yb_N and Eu/Eu* values of the *Xiashu* loess span the equivalent ranges for the CLP deposits but they have a much greater degree of variability. The variation of these REE parameters of *Xiashu* loess samples in the three zones (Fig. 6), defined according to spatial changes in the values of TiO_2/Al_2O_3 and SiO_2/Al_2O_3, is discussed below, with reference to Fig. 8. The <20 μm fractions of the Yangtze River and the Yellow River sediments also have a REE distribution pattern typical of the UCC, overall similar REE parameters, and they only partially overlap with the *Xiashu* loess on plots of Eu/Eu* vs. LREE/HREE and Gd_N/Yb_N vs. La_N/Sm_N (Fig. 6).

The high field strength elements (Zr, Hf, Nb, Ta, Th, Y and Sc) and their ratios are valuable for inferring provenance because of their immobility during chemical weathering (Taylor and McLennan, 1985; Condie, 2005). The <20 μm fraction of the *Xiashu* loess samples can be clearly distinguished from that of the CLP eolian deposits in the plots of the trace element ratios (Fig. 7). Compared with the CLP samples, the *Xiashu* loess samples generally have high ratios of La/Sc, Th/Sc, Zr/Sc, Zr/Hf and Nb/Ta, and low ratios of Y/Nb and La/Nb. Furthermore, the *Xiashu* loess samples typically have a wider range of trace element ratios than the CLP and river sediment samples; this is more clearly evident in the ranges of La/Sc (1.98–5.21), Th/Sc (0.73–1.51), Zr/Sc (9.40–25.96) and Nb/Ta (13.30–15.90). The variation of these trace element ratios of *Xiashu* loess samples in the three zones (Fig. 7), defined according to spatial changes in the values of TiO_2/Al_2O_3 and SiO_2/Al_2O_3, is discussed below, with reference to Fig. 9. The distribution for the Yangtze River sediments only partially overlaps with that of the *Xiashu* loess (Fig. 7). The Yellow River sediments plot close to those of the Yangtze River and are distinct from the CLP loess samples, which suggests that the Yellow River sediments are a mixture of eroded loess and bedrock debris from the drainage area.

The spatial changes in most of the REE and trace element ratios of the *Xiashu* loess (Figs. 8 and 9) show a similar distribution to those of the major element ratios (Fig. 5). LREE/HREE (Fig. 8a) has the most clearly defined spatial distribution. In Zone I, three sites have values < 11.00, with one outlier (section 3) with a value of 12.25. In Zone II, most of the sites have values within the range of 11.41–13.63; and one outlier (section 13), located in northernmost of the zone, has a value of 9.80. In Zone III, the three eastern sites (sections 18–20) have values ranging from 10.43 to 10.98, and the two western sites (sections 21 and 22) have values > 11.00. The Yellow River sediment sample has a value of 8.86, and the Yangtze River sediments have values ranging from 8.64 to 9.77.

The La_N/Sm_N ratios of the *Xiashu* loess exhibit only a weak spatial pattern (Fig. 8b). In Zone I, the three sites have La_N/Sm_N values < 4.60, with one outlier (section 3) with values up to 4.74. In Zone II, most of the sections have La_N/Sm_N values ranging from 4.61 to 4.83, and only the two northernmost sites (sections 13 and 14) have values < 4.50. In Zone III, the three eastern sites have La_N/Sm_N values < 4.60, while the two western sites have values of 4.78 and 4.91, respectively. The La_N/Sm_N ratio of the Yellow River sediment sample is 4.29, and the Yangtze River sediments have a narrow range of values (4.35 and 4.63) which is higher than that of the Yellow River, and overall lower than loess in Zone II.

These spatial patterns are not evident in the Eu/Eu* and Gd_N/Yb_N ratios (Fig. 8c and d). Eu/Eu* has a different spatial pattern to the other ratios. The sites with high Eu depletion (Eu/Eu*<0.64) are mostly located close to the Dabie Mts. The Eu/Eu* value of the Yellow River sediments is 0.68 and those of the Yangtze River sediments have a narrow range (0.68–0.70). The Gd_N/Yb_N ratio of the *Xiashu* loess ranges from 1.22 to 1.75. The Yellow River sediment has a Gd_N/Yb_N value of 1.32 and the Yangtze River sediments have Gd_N/Yb_N values ranging from 1.25 to 1.39.

The spatial pattern of changes in trace element composition are best seen in the plots of Zr/Sc and Th/Sc (Fig. 9a and b). They show a spindle-shaped pattern with a NW-SE orientation, similar to that of TiO_2/Al_2O_3. In Zone I the loess sections have Zr/Sc values < 13.00; in Zone II the loess sections have Zr/Sc values > 14.00 (range of 14.09–20.24); and in Zone III, the three eastern loess sections have Zr/Sc values ranging from 10.88 to 11.11, while those of the two western loess sections have higher values (14.47 and 16.20). The Yellow River sediment sample has a Zr/Sc value of 12.44 and the Yangtze River sediments have Zr/Sc values ranging from 10.94 to 13.01. For the Th/Sc ratio, Zone I has values < 0.90; Zone II has values > 0.90 (0.90–1.37), and only section 13 in the northernmost part of this zone has a value of 0.78; and in Zone III the three eastern

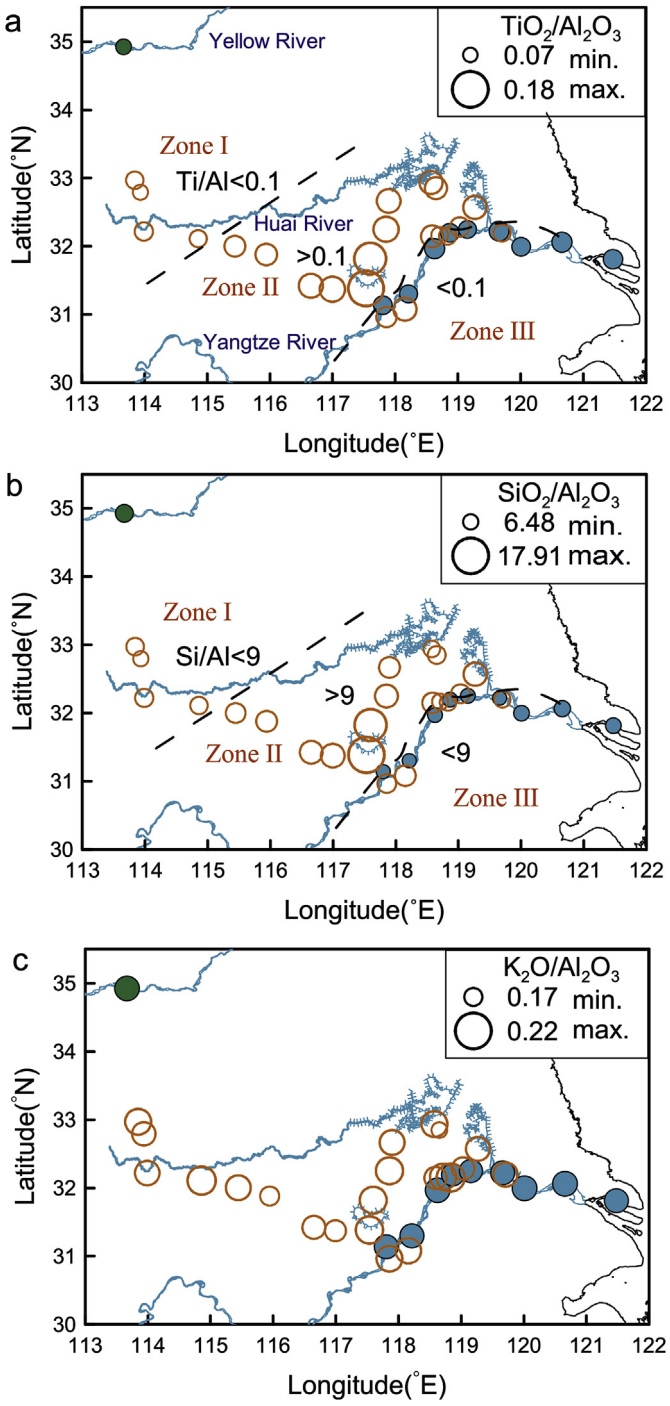

Fig. 5. Distribution of major element ratios of the *Xiashu* loess and the river sediments. (a) TiO_2/Al_2O_3, (b) SiO_2/Al_2O_3, (c) K_2O/Al_2O_3. The open circles are loess data and the solid circles are river sediments data; the size of the circles is proportional to the value of the ratio. The dashed lines in Fig. 5a and b represent the boundaries between the geochemical zones.

sections have values ranging from 0.80 to 0.83, while the two western loess sites have higher values of 0.90 and 0.91. The Yellow River sediment sample has a Th/Sc ratio of 0.71, and the values of the Yangtze River sediments range from 0.76 to 0.82.

In contrast to Zr/Sc and Th/Sc, the Y/Nb and La/Nb ratios are relatively low in Zone II (Fig. 9c and d). In Zone I, two of the four loess sections have Y/Nb values > 0.80; in Zone II the loess sections generally have low Y/Nb values (0.64–0.72), with the exceptions of section 12 in the north and section 9 in the south, with values of 0.79 and 0.54, respectively; and in Zone III, the three eastern sections have relatively high Y/Nb values (0.78–0.83), while the two western loess sections have relatively low values (0.72 and 0.73). The Yellow River sediment sample has a Y/Nb value of 1.19, while the Yangtze River sediments have relatively low values (0.90–1.08). For La/Nb, 3 of the 4 loess sections in Zone I have values > 1.50; Zone II has overall lower values (1.28–1.65); and in Zone III, the three eastern loess sections have relatively high values (1.69–1.78), while the two western sites have relatively low values (1.34 and 1.49). The Yellow River sediment sample has a La/Nb ratio of 1.96, and the Yangtze River sediments have relatively low values (1.67–1.78).

There is no distinct zonal pattern of changes in Nb/Ta and Zr/Hf ratios (Fig. 9e and f). Zones I and II have Nb/Ta ratios of 13.73–14.97; and in Zone III, the three eastern sections have Nb/Ta ratios of 13.70–13.94, while the two western sections have values of 13.86 and 14.54. The Yellow River sediment sample has a relatively low Nb/Ta ratio of 13.14, while the Yangtze River sediments have relatively high Nb/Ta ratios (13.78–14.08). The *Xiashu* loess sections have Zr/Hf ratios ranging from 40.46 to 43.64; the Yellow River sediment sample has a relatively low Zr/Hf ratio of 39.84; and the Yangtze River sediments have slightly higher Zr/Hf ratios (40.73–42.21).

Notably, in Zone III, the three eastern loess sections have trace element (including REE) compositions close to those of the Yangtze River sediments, while the compositions of the two western loess sections are close to those of those of the neighboring sections to the north of the Yangtze River. Zone I has a composition close to that of the Yellow River sediments, while Zone II has a distinctly different composition to that of the Yellow River sediments.

4. Discussion

4.1. Evaluation of the effect of post-depositional weathering on the geochemical composition of loess

The geochemical composition of loess is influenced by the source material, sediment sorting during wind transport, and post-depositional pedogenesis and chemical weathering. In this study, we use the <20 μm fraction for geochemical analysis largely to reduce the influence of grain-size sorting during transport. However, the influence of post-depositional weathering needs to be evaluated to provide a basis for determining the original geochemical composition of the source material of the *Xiashu* loess deposits.

As indicated by the CIA values and the A-CN-K ternary diagram (Fig. 3), the <20 μm fraction of the Last Glacial *Xiashu* loess from the 22 loess sections has undergone moderate weathering strength, with a wide range of CIA values from 64.48 ± 1.46 (section 10) to 75.14 ± 0.71 (section 22). A wide range of CIA values have also been reported by previous studies, which show that bulk loess samples from the Zhenjiang section (close to section 18) have CIA values < 70 (Yang et al., 2004; Zhang et al., 2007), and that bulk loess samples from the Xuancheng and Jiujiang sections have CIA values ranging from 78 to 88 (Qiao et al., 2011). The strong alteration of the glacial loess in the latter two sections may be partly caused by the downward penetration of the effects of pedogenesis within the overlying paleosols. In our study, although the most weathered sections (sections 21 and 22 in Zone III, with CIA = 74.13 ± 0.35 and 75.14 ± 0.71, respectively) lie at the southeastern part of the studied region, the least weathered sections (sections 9, 10 and 11 in Zone II, with CIA = 64–66) are located in the region between the Yangtze River and the Huai River (Fig. 1). Notably, 10 of the 22 sections have CIA values even lower than that

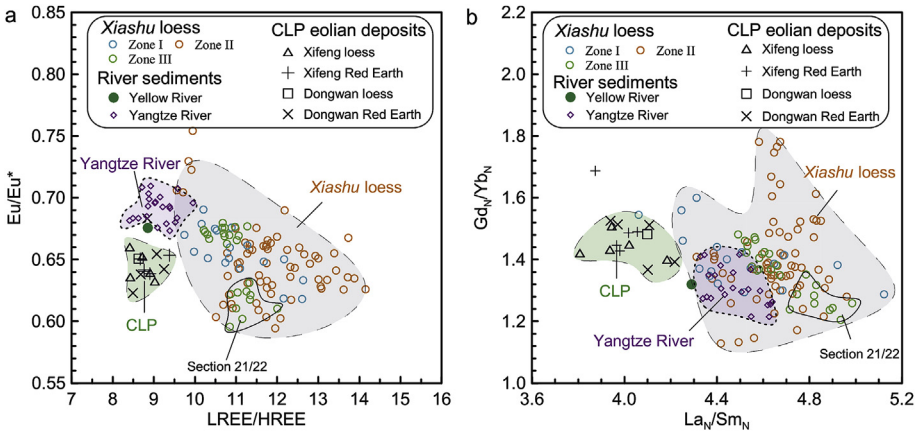

Fig. 6. Plots of (a) Eu/Eu* vs. LREE/HREE, (b) Gd_N/Yb_N vs. La_N/Sm_N for the <20 μm fraction of the *Xiashu* loess, CLP eolian deposits and the river sediments. The *Xiashu* loess samples are shown by three different colored symbols according to three zones defined by spatial changes in SiO_2/Al_2O_3 and TiO_2/Al_2O_3 ratios of the *Xiashu* loess shown in Fig. 5.

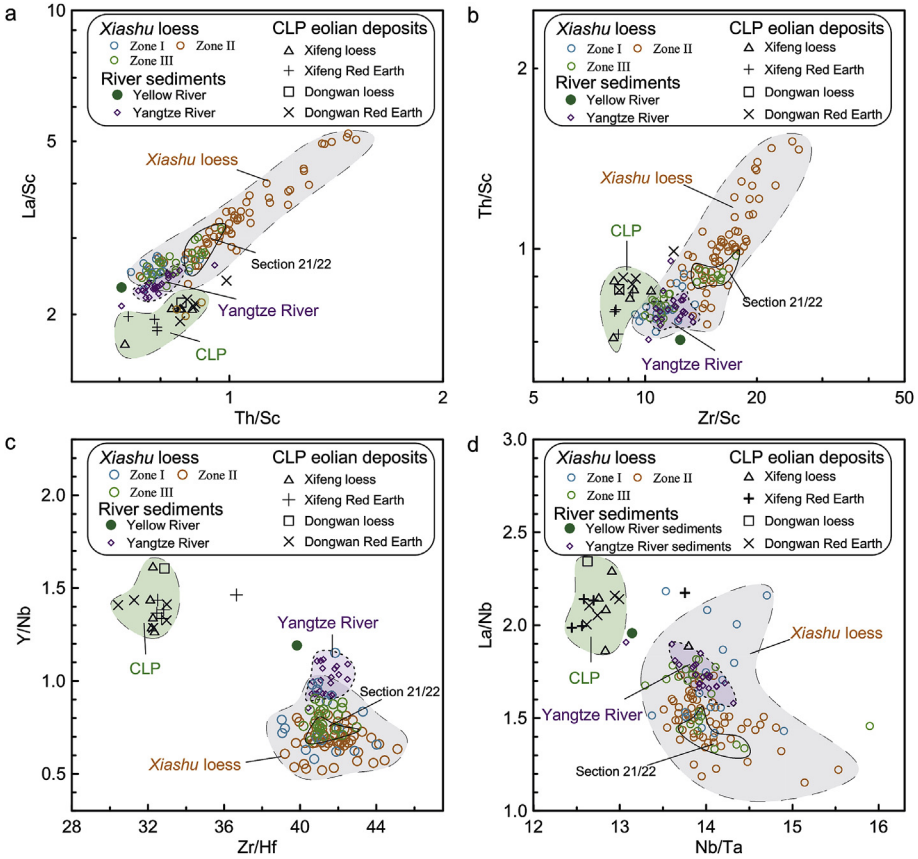

Fig. 7. Plots of (a) La/Sc vs. Th/Sc, (b) Th/Sc vs. Zr/Sc, (c) Y/Nb vs. Zr/Hf and (d) La/Nb vs. Nb/Ta for the <20 μm fraction of the *Xiashu* loess, CLP eolian deposits and the river sediments. The *Xiashu* loess samples are shown by three different colored symbols according to three zones defined by spatial changes in SiO_2/Al_2O_3 and TiO_2/Al_2O_3 ratios of the *Xiashu* loess shown in Fig. 5.

of the L1 loess of the Xifeng section (CIA = 69.27 ± 1.33) in the central CLP (Tables S1 and S2). This phenomenon is also illustrated in Fig. 3 that many samples of the *Xiashu* loess have lower CIA values than the CLP eolian deposits. It would be expected that, during glacial periods, there was a weak southwards-increasing trend of temperature and precipitation from the CLP to the southern loess region. The fact that no comparable weathering trend is evident for the glacial loess suggests that the CIA values were mainly inherited from the source material rather than being the product of post-depositional weathering.

Under incipient to intermediate weathering conditions, SiO_2, Al_2O_3, TiO_2 and K_2O are relatively resistant to chemical weathering (Nesbitt and Wilson, 1992; Condie et al., 1995), and hence the ratios of TiO_2/Al_2O_3, SiO_2/Al_2O_3 and K_2O/Al_2O_3 are useful for reflecting the mineralogy and geochemistry of the dust sources (Sheldon and Tabor, 2009; Hao et al., 2010; Peng et al., 2016). K-feldspar is more resistant to chemical weathering than plagioclase, and during the weathering of K-bearing silicates, part of the K is tightly bound

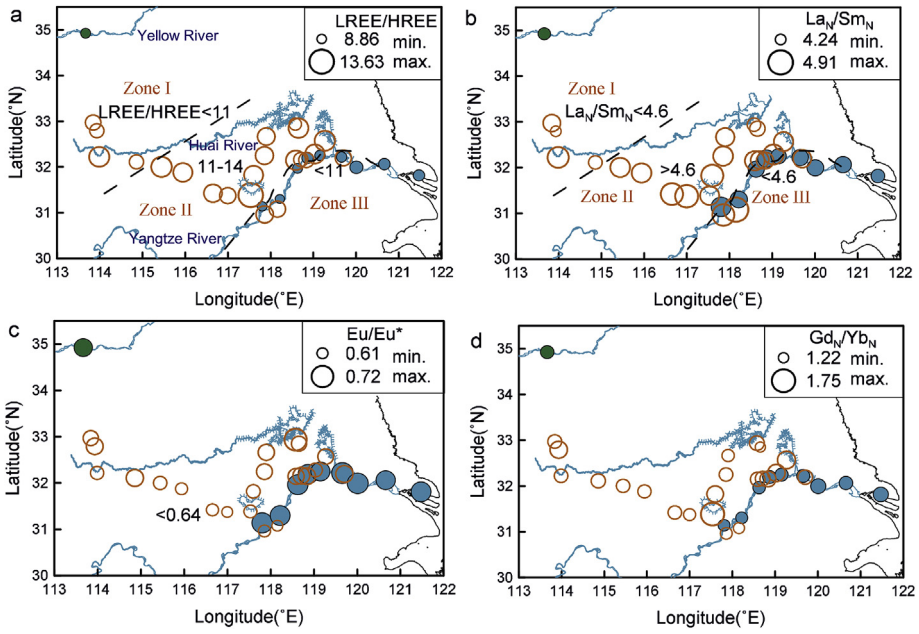

Fig. 8. Spatial distribution of REE ratios of the *Xiashu* loess and the river sediments. (a) LREE/HREE, (b) La_N/Sm_N, (c) Eu/Eu*, (d) Gd_N/Yb_N. The format is the same as in Fig. 5.

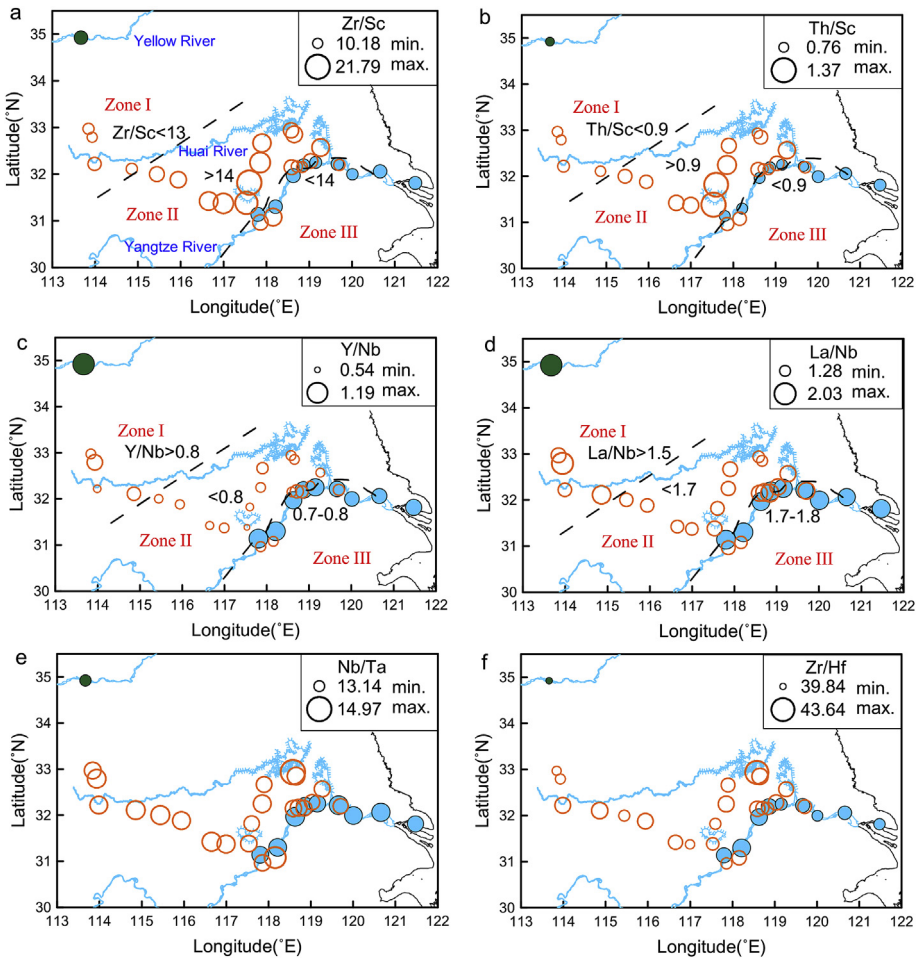

Fig. 9. Spatial distribution of immobile trace element ratios for the *Xiashu* loess and the river sediments. (a) Zr/Sc, (b) Th/Sc, (c) Y/Nb, (d) La/Nb, (e) Nb/Ta and (f) Zr/Hf. The zonal division and the symbols are the same as Fig. 5.

in the illite clay lattice. However, elemental K may be slightly leached under intermediate weathering conditions. Si is less mobile than K because quartz is more resistant to chemical weathering than feldspar. Ti and Al may remain unaffected under moderate to intensive chemical weathering, because Al and Ti have the lowest solubility in natural water of all the major elements (Broecker and Peng, 1982; Sugitani et al., 1996). The evidence outlined below supports the conclusion that the elements K and Si are relatively immobile in the studied samples. The weathering trend of our samples does not evolve along the A-K boundary in the A-CN-K ternary diagram (Fig. 3), and the K_2O/Al_2O_3 ratios are relatively uniform (~0.20) for most of the sections in the spatial distribution diagram (Fig. 5c). The SiO_2/Al_2O_3 ratios increase southward in the region between the Huai River and the Yangtze River (Fig. 5b and c). If post-depositional weathering has had an effect, the SiO_2/Al_2O_3 ratios would have shown a southwards decrease, because chemical weathering preferentially leads to removal of Si compared with Al (Nesbitt and Muir, 1988). The absence of a southwards-decreasing trend of the two ratios of K_2O/Al_2O_3 and SiO_2/Al_2O_3 indicates that post-depositional weathering was not the dominant factor responsible for their changes, and thus the ratios of TiO_2/Al_2O_3, SiO_2/Al_2O_3 and K_2O/Al_2O_3 can be used as a dust source indicator.

The rare earth elements, from La to Lu, occur in both heavy and light minerals (amphiboles, micas, zircon, chlorite, clay minerals, apatite, and even trace amounts in feldspars) (Taylor et al., 1983). Thus, the REE can potentially reflect both proximal and distal loess sources (Muhs and Budahn, 2006). Although REE elements are usually relatively immobile, there is evidence showing that HREE are mobilized to a greater extent than are the LREE under strong weathering (Nesbitt, 1979). However, the results of REE analyses of the Xuancheng and Jiujiang loess (Qiao et al., 2011) and Zhenjiang loess (Li et al., 2006) indicate indistinguishable REE fractionation between paleosol and loess layers. The vermiculated Red Soil beneath the *Xiashu* loess in the Xuancheng and Jiujiang sections, which formed in extremely wet and warm interglacials, also has similar REE ratios to the overlying *Xiashu* loess (Qiao et al., 2011). These various lines of evidence show that REE are immobile in the eolian deposits of southern China, even during interglacial periods. The immobile nature of the REE in our studied samples is also demonstrated by the absence of a spatial gradient throughout the studied *Xiashu* loess region. In previous provenance studies of eolian deposits, the REE indices have been used successfully (Muhs and Budahn, 2006; Muhs et al., 2007; Yang et al., 2007a, b; Hao et al., 2010; Hu and Yang, 2016; Liu and Yang, 2018).

Zr, Hf, Nb and Ta are mainly carried by weathering-resistant minerals, which leads to unchanging Zr/Hf and Nb/Ta ratios, even under intensive weathering (Condie et al., 1995; Kurtz et al., 2000; Kahmann et al., 2008). Sc is immobile in early to intermediate weathering conditions (Brown et al., 2003) and is readily adsorbed by clays during intensive weathering (Loring, 1991; Marques et al., 2004). Ratios such as Th/Sc and La/Sc are significantly different in felsic and basic rocks (Taylor and McLennan, 1985; Bhatia and Crook, 1986; Cullers et al., 1988). Nb/Ta ratios, and the fractionation of Nb from REE, such as is indicated by La/Nb and Y/Nb, are critical for understanding magmatic processes and protolith characteristics (Winchester and Floyd, 1977; Eby, 1990; Condie, 2005). All of the above trace element ratios have been successfully used as provenance indicators (Condie, 2005; Muhs and Budahn, 2006; Muhs et al., 2007; Liu and Yang, 2013; Ren et al., 2014). In our study, zonal changes in the element ratios, in the absence of a uniform gradient, also confirm the immobile nature of these trace elements. From the foregoing analysis, we conclude that for the *Xiashu* loess the geochemical indices derived from these immobile elements are not significantly altered by post-depositional chemical weathering.

4.2. Contrast in geochemical homogeneity between the Xiashu loess and the loess of the Chinese Loess Plateau

Evaluation of the effects of post-depositional weathering on the geochemical composition of the studied samples leads us to conclude that the element ratios and REE parameters mainly reflect the original geochemical composition of the dust that forms the *Xiashu* loess. Comparison of eolian deposits between the CLP and the northern subtropical region reveals a pronounced contrast in geochemical homogeneity. The eolian deposits of the CLP have a relatively uniform geochemical composition. The Xifeng and Dongwan sections are located in the central and western CLP, respectively, and samples from these sections span the interval from the late Miocene to the late Pleistocene. Despite their large temporal and spatial coverage, these CLP deposits exhibit a restricted range of major and trace element ratios and REE parameters (Figs. 4, 6 and 7). This is consistent with previous studies indicating that the CLP loess is derived from dust sources in the deserts of the Asian interior and that its provenance has not changed significantly since the late Cenozoic (Liu et al., 1994; Guo et al., 2001, 2002; Jahn et al., 2001; Sun, 2002; Chen et al., 2007; Che and Li, 2013; Chen and Li, 2013; Li et al., 2018). By contrast, the *Xiashu* loess has a striking geochemical heterogeneity, which is evident throughout a wide range of major, trace element ratios and REE parameters (Figs. 4, 6 and 7). This heterogeneity is also illustrated by the zonal changes in TiO_2/Al_2O_3, SiO_2/Al_2O_3, LREE/HREE, La_N/Sm_N, Zr/Sc, Th/Sc, La/Nb and Y/Nb (Figs. 5, 8 and 9) and by the absence of a uniform gradient, both between the composition zones and within the composition zones themselves. This absence of a uniform gradient is also one form of evidence demonstrating that sedimentary sorting was not the dominant factor responsible for the observed inter-site variability in geochemical composition.

A further evaluation of the contrast in the homogeneity of the geochemical composition of the *Xiashu* loess and CLP loess is presented in Fig. 10, which shows plots of SiO_2/Al_2O_3 vs. TiO_2/Al_2O_3. In this figure, the bulk samples and the <20 μm fraction samples are used to evaluate spatial changes in the geochemical composition of the CLP loess deposits. The bulk sample data include the samples from the NW-SE and W-E transects (spanning ~320 km and ~620 km, respectively, see Fig. 1b); and samples from the Xining, Xifeng and Jixian sections, which consist of another W-E transect of ~800 km length (Jahn et al., 2001). Of these two element ratios, TiO_2/Al_2O_3 remains constant between different fractions of silt-sized particles in the well-mixed CLP loess deposits (Gu, 1999); however, the values are lower in the clay fraction, which may be caused by the resistance of Ti-bearing minerals to weathering which prevents their comminution into clay-sized particles. By contrast, the SiO_2/Al_2O_3 ratios have a positive relationship with particle size within the clay and silt fraction, therefore the SiO_2/Al_2O_3 ratio of the bulk samples was influenced by sedimentary sorting (Peng and Guo, 2001; Hao et al., 2010). The most striking feature of the data is that although the samples from the CLP are distributed across a vast region, both ratios show a rather restricted range of values. In the CLP, the bulk samples have higher SiO_2/Al_2O_3 ratios than the <20 μm fraction, due to the fact that the coarse fraction of the bulk samples is enriched in quartz. The high TiO_2/Al_2O_3 ratio of the bulk samples is because the clay fraction, with lower TiO_2/Al_2O_3 ratios, represents a smaller proportion of the bulk samples than is the case of the <20 μm fraction. The restricted range of geochemical composition of the CLP indicate that spatial changes in the two ratios are minor in the context of the overall uniformity of the dust sources of the deserts of the Asian interior. However, the *Xiashu* loess show wide range of the two ratios (Fig. 10). This further shows the contrast in geochemical homogeneity between the *Xiashu* loess and the CLP loess.

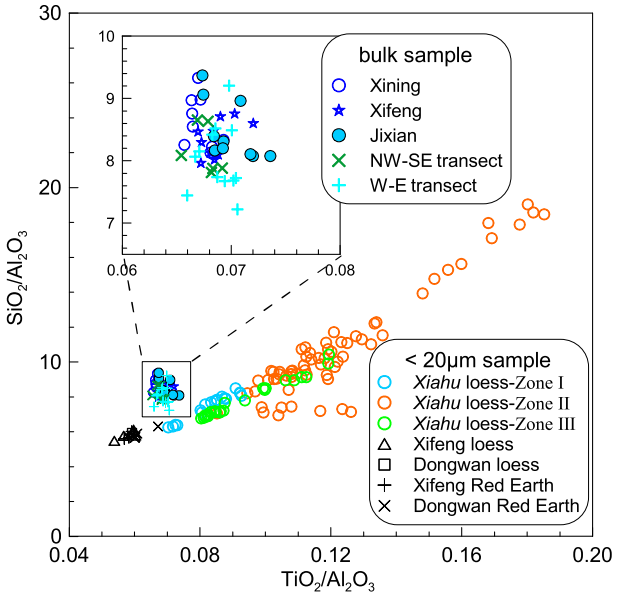

Fig. 10. Plot of SiO_2/Al_2O_3 vs. TiO_2/Al_2O_3 for the bulk samples of CLP loess along two transects, and the <20 μm fraction of the *Xiashu* loess and CLP eolian deposits. The bulk samples are from the L1 and S1 layers on the NW-SE and W-E transects across the CLP (Fig. 1b). The Xining, Xifeng and Jixian data are cited from Jahn et al. (2001). Note the remarkably wide ranges of SiO_2/Al_2O_3 and TiO_2/Al_2O_3 ratios for the *Xiashu* loess compared with the CLP loess. The *Xiashu* loess samples are shown by three different colored symbols according to three zones defined by spatial changes in SiO_2/Al_2O_3 and TiO_2/Al_2O_3 ratios of the *Xiashu* loess shown in Fig. 5.

This difference in homogeneity between the eolian deposits of the two regions provides important information about the transport processes of the dust forming the deposits. It is well accepted that the dust deposited in the CLP was transported for at least hundreds of kilometers, and thus it is reasonable to conclude that the homogeneity of the CLP loess is an intrinsic feature of relatively long-distance transported, well-mixed dust. If the *Xiashu* loess had also been a mainly long-distance transported eolian deposit, the long-distance transported dust would have distributed across a wide region, which would have led to a homogeneous geochemical composition of the dust deposits on a large spatial scale. Thus, the significant heterogeneity of the *Xiashu* loess undoubtedly indicates that the *Xiashu* loess has no uniform dust source region, or that the dust source region was spatially heterogeneous in composition, and that the dust was only transported over a short distance.

4.3. Differences in the source of the Xiashu loess and the CLP loess

The *Xiashu* loess and the deposits of the CLP fall within different composition fields defined by major, trace element ratios and REE parameters (Figs. 4, 6, 7 and 10). Because the CLP loess broadly reflects the average composition of deserts in the Asian interior, and the geochemical indices in turn reflect the composition of this source material, it is evident that the dust forming the *Xiashu* loess did not come from the northern deserts. Nevertheless, this conclusion is seemingly contradicted by observations of modern dust storms. Modern meteorological data show that the southern edge of dust storms reaches the latitude of 30°N in southern China and the marginal seas of China and beyond (Uno et al., 2004; Shao and Dong, 2006; Tan et al., 2017). In southern China, wet deposition accounts for a large proportion of the floated high-level dust (Zhao et al., 2003), and the observed 'rain dustfall' in Nanjing city on March 11, 2006 had a chemical composition which is more similar to the CLP loess than to the local *Xiashu* loess (Li et al., 2009b). These observations were often used as evidence for the northern desert origin of the *Xiashu* loess. However, it can be expected that during glacial periods the dust storms would be stronger than those of the present day. If the dust from the northern deserts dominated the composition of the *Xiashu* loess, at least some of the samples of the *Xiashu* loess would be expected to have a similar geochemical composition to that of the CLP loess. However, the distinctive composition of the *Xiashu* loess compared to the CLP loess suggests that in the geological past the deserts of the Asian interior never made a major contribution to the dust forming the *Xiashu* loess.

During most (~90%) of the dust storms in the northern deserts, dust particles from the Gobi deserts are usually entrained in the lower atmosphere (<3 km altitude) and a large amount of dust is deposited in regions such as the CLP (Sun et al., 2001; Sun, 2002). Dust transport is also affected by geomorphological factors. The Qingling Mts., forming the southern boundary of the CLP, reach elevations above 2 km. According to a modeling simulation, one high concentration center of mineral dust aerosols emerges to the north of the Qingling Mts. in the spring season, due to the blocking effect of the complex terrain (Wu et al., 2005). In order to assess the influence of the southward transport of northern dust on the *Xiashu* loess, we studied four loess sections from two major basins (Luonan Basin and Shangdan Basin) in the eastern Qinling Mts. (Li et al., 2016), which lie on the pathway of northern dust storms. The immobile element ratios of the <20 μm fraction (TiO_2/Al_2O_3, La_N/Sm_N, Gd_N/Yb_N, La_N/Yb_N, Eu/Eu^*, Zr/Nb, Hf/Nb, Y/Nb, La/Nb, Th/Nb, Ta/Zr, Zr/Hf, Y/Ho, Al/Nb, Ti/Nb, Zr/Ti and Zr/Al) of the loess deposits from the eastern Qinling Mts. are different from those of the CLP loess (Li et al., 2016). This finding agrees with the results of analysis of the elemental and Sr-Nd isotopic composition of other loess sections in the eastern Qinling Mts. (Zhang et al., 2012; Fang et al., 2017). The clear distinction in the geochemical composition between samples from the two regions indicates that the loess deposits in the eastern Qinling Mts., located between the CLP and the *Xiashu* loess region, are not sourced from the northern deserts, which is further evidence supporting the conclusion that the *Xiashu* loess is not primarily derived from the deserts of the Asian interior deserts.

4.4. Dominance of a local dust source for the Xiashu loess

A local source of the *Xiashu* loess was proposed in several previous studies. The proposed loess dust source regions include the Yangtze River valley and adjacent lake beds, or the continental shelf (e.g. Yang, 1986; Zhao and Li, 1990; Qiao et al., 2003). Yang (1986) proposed that during the Last Glacial Maximum the exposed sediments of the Yangtze River, and of the lakes on both sides of the river, were dust sources for the *Xiashu* loess. As early as the 1990s, the exposed continental shelf, more specifically the North Jiangsu shoal area, was proposed as a dust source for the *Xiashu* loess (Zhao and Li, 1990). However, this view was soon replaced by the view that the occurrence of the *Xiashu* loess resulted from southward incursion of the CLP loess which was derived from the northern deserts (Liu, 1985; Yang, 1991). It is till to the early 2000s when there occurred a revival of the concept of a proximal source of the *Xiashu* loess (Qiao et al., 2003). The study is based on the presence of significant proportions of particles coarser than 32 μm which are unlikely to have been transported for a long distance, together with a reinterpretation of the geochemical composition (Qiao et al., 2003). Subsequently, Hao et al. (2010) used observed differences in major and trace element composition of the <20 μm fraction between the loess in the Yangtze River valley and that of the CLP loess to conclude that *Xiashu* loess in the Yangtze River valley was not sourced from the northern deserts. In fact, the earliest mineral and geochemical evidence has long been ignored, including the

similarity of mineral assemblages of the *Xiashu* loess to the suspended sediments of the Yangtze River (Yang, 1986), and differences in the $\delta^{18}O$ of quartz between the *Xiashu* loess and the CLP loess (Gu, 1987). Recent provenance studies using detrital zircon U-Pb age spectra revealed similar zircon signals of the *Xiashu* loess in the lower Yangtze River valley to those of the fluvial sediments (Liu et al., 2014; Wang et al., 2017; Qian et al., 2018).

In addition, Hao et al. (2010) noticed that the main distribution of loess in southern China was in the region north of the Yangtze River, and they suggested that the alluvial plain was possibly an important source for the *Xiashu* loess. In a recent study of a borehole loess section in the Chaohu lake basin (close to section 10), values of CIA, Na/K and SiO_2/Al_2O_3 were used to suggest that the well-developed alluvial-lacustrine deposits in the Huai River floodplain were the major source of the loess (Guan et al., 2016). However, another study, based on element enrichment factors (Kemp et al., 1976) in a loess section in the upper reaches of the Huai River (close to section 4), concluded that the eolian deposits were sourced from the northern deserts (Zhang and Song, 2013). Thus, a systematic investigation of the provenance of loess in the northern *Xiashu* loess region is necessary to reconcile these different views.

The present study has used geochemical evidence from seventeen sections covering most of the northern *Xiashu* loess region to conclude that the loess deposits in the region were not derived from the deserts of the Asian interior. This leaves several potential local sources to be considered: the continental shelves of the East China seas, the valleys of the Yangtze River and Yellow River, and the alluvial plain of the Huai River. The sediments on the continental shelf are the result of the transport by tidal currents of sediments from the Yellow or Yangtze rivers, and the erosion of late Pleistocene material on the seabed (Zhu and Chang, 2000). However, according to the biplots of element ratios (Figs. 4, 6 and 7), the sediments of the Yellow River and Yangtze River have a restricted range of geochemical composition compared to the *Xiashu* loess. Clearly, the continental shelf sediments, which are mainly a mixture of two endmembers of sediments supplied by the Yellow River and Yangtze River, cannot explain the observed wide range in geochemical composition of the loess in the northern *Xiashu* loess region (Figs. 5, 8 and 9). In addition, the significant spatial heterogeneity of the *Xiashu* loess does not support the concept of a single dust source. Thus, we conclude that continental shelf sediments are not the main source of the *Xiashu* loess in the northern *Xiashu* loess region.

The high degree of variability of the geochemical composition of the northern *Xiashu* loess suggests the existence of multiple sources. Below, we explore the contribution of the sediments of the Yangtze River and the Yellow River and the alluvial plain of the Huai River to the *Xiashu* loess. In the upwind region of Zone I, dust supplied from the Yellow River floodplain was recorded in the proximal loess to the south of the Yellow River (Zheng et al., 2007; Prins et al., 2009; Shang et al., 2018). This was attributed to the funneling of dust-bearing winds along a canyon of the Yellow River (Porter, 2001). In Zone I, the *Xiashu* loess has lower values of TiO_2/Al_2O_3, SiO_2/Al_2O_3 (Fig. 5a and b), Zr/Sc, Th/Sc and Zr/Hf (Fig. 9a, b and f), and higher values of La/Nb and Y/Nb (Fig. 9c and d); notably, the values also plot close to those of the Yellow River sediments. Thus, we infer that both the Yellow River floodplain and Huai River alluvial plain potentially make an important contribution to the *Xiashu* loess in Zone I.

In Zone II, between the Huai River and the Yangtze River, the geochemical composition (e.g. TiO_2/Al_2O_3, SiO_2/Al_2O_3, Zr/Sc, Th/Sc and Zr/Hf) of the *Xiashu* loess is distinct from that of the Yellow River sediments. This precludes the possibility that the floodplain of the Yellow River is the main dust source for the loess of Zone II. Hence, the evidence presented herein suggests that the local alluvial plain in the present Huai River drainage is likely the main source of the *Xiashu* loess in Zone II. Yu (1999) suggested that the purple-red clay of Paleogene-Neogene age in northern Jiangsu was a potential dust source for the *Xiashu* loess. Silt-sized particles can be produced by high-altitude erosional processes (Assallay et al., 1998), and loose materials on the nearby mountains, with different parent rock types, could also be the dust source of the *Xiashu* loess. The significant heterogeneity of the geochemical composition of the *Xiashu* loess in Zone II is tentatively attributed to the corresponding heterogeneity of the geochemical composition of the sediments in various geomorphological settings of the Huai River alluvial plain.

In Zone III, the source of the loess deposits depends on the local geographical and geomorphological context. Our study has revealed the remarkable homogeneity of the major, REE and trace element ratios of the fluvial sediments in the lower reaches of the Yangtze River, as illustrated by the spatial distributions shown in Figs. 5, 8 and 9. The three eastern loess sections (sections 18–20) have values close to those of the Yangtze River sediments, indicating that these sediments were the dust source for the loess in these regions. By contrast, the two western loess sections (sections 21 and 22) have trace element ratios close to those of the neighboring sites to the north of the Yangtze River. Observation shows that sections 21 and 22 are located in a wind gap between the Dabie Mts. and the Zhangba Hills (Fig. 1c). Therefore, it is possible that dust sources from both north of the Yangtze River and the Yangtze River valley contribute to the dust deposits of these two sections.

However, it seems impossible for the 'Yangtze River dust' to be transported northwards to the extensive loess deposits in the northern *Xiashu* loess region (Zones I and II) because of the prevailing northerly winter winds which are the principal dust carrier (Zhang et al., 1997). On the other hand, even if a paleochannel of the Yangtze River meandered on a large scale in the geological past (Yang, 1986; Li et al., 2002), the Dabie Mts. and the Zhangba Hills are barriers that would block its northward movement. Therefore, the Yangtze River sediments cannot have contributed to the loess of Zone II, as confirmed by the distinct geochemical composition of the Yangtze River sediments. As shown in the biplots of provenance indices (Figs. 4, 6 and 7) and the maps of the distribution of element ratios (Figs. 5, 8 and 9), the Yangtze River sediments only partly overlap with the *Xiashu* loess.

4.5. Intensified aridity in northern subtropical China during glacial times

There are three fundamental requirements for loess formation: (1) a sustained source of dust, (2) sufficient wind energy to transport the dust, and (3) a suitable accumulation site (Pye, 1995). The deposition of loess deposits is usually regarded as an indicator of an arid climate with low vegetation coverage in the dust source region. The long-held view of the formation of the *Xiashu* loess is that it is related to intensified aridification in the deserts of northern China and a strengthened winter monsoon (Liu, 1985). An alternative view is that the formation of the *Xiashu* loess resulted from the aridification of valleys of the Yangtze River and its tributaries during glacial periods. This is broadly similar to the case of eolian deposits adjacent to large rivers worldwide (Smalley et al., 2009). A revised hypothesis of a local dust source is that the *Xiashu* loess is indicative of environmental conditions on the alluvial plain north of the Yangtze River, based on the evidence of the major loess distribution region to the north of the Yangtze River (Hao et al., 2010). Our geochemical evidence from the seventeen loess sections from the vast northern *Xiashu* loess region supports this hypothesis.

The dominance of local sources for the widespread loess deposits in the northern *Xiashu* loess region revealed by this study points to intensified aridity in the region of northern subtropical China between the Qinling Mts. and the Yangtze River during glacial times. During glacials, the alluvial plain should have been sufficiently arid to provide significant amounts of dust to form the loess deposits. Although there were no large areas of deserts, like those in the Asian interior, a mosaic of desert-like landforms may have existed.

The aridification of the northern subtropical region was closely linked with a decrease in sea level and decrease in the strength of the East Asian summer monsoon, which were initially driven by the increased volume of ice sheets mainly in northern high latitudes. During MIS 2–4, the fall in sea level was up to 50–125 m (Rohling et al., 1998, 2009), which would have had several consequences. First, the coastline in the eastern China seas would have retreated eastwards by 6–7° longitude, resulting in the exposure of a large shelf area in eastern Asia, and the fall in sea level would also have led to the exposure of a large shelf area in Southeast Asia during the Last Glacial Maximum (Wang, 1999). This would have significantly increased the continentality of the present northern subtropical region. Second, retreat of the coastline would have increased the distance from the oceanic moisture source, thus weakening the summer monsoon. Third, the fall in sea level would have led to a decrease in the level of the groundwater table and in the water level of lakes and rivers. The further weakening of the East Asian summer monsoon in glacials (Hao and Guo, 2005) would also have been promoted by several additional factors: the southward displacement of climate zones due to the huge continental ice sheets in the Arctic region; the prolonged residence of the subtropical jet south of the Tibetan Plateau, inhibiting the northward penetration of the East Asian summer monsoon (Pullen et al., 2011); and the shortening of the summer season due to the strengthened winter monsoon and the prolonged winter-half year (Wang et al., 2018). These various changes, forced by the decrease in sea level and the weakening of the summer monsoon, would have led to a decrease in vegetation density, which would have exerted a positive feedback effect and reinforced the aridity. Notably, a pollen study has revealed that the vegetation of the studied region was dominated by herbaceous plants during glacials (Shao, 1988).

Due to the eastward retreat of the river mouth, the channel would have been deeply incised. A decrease in the level of lakes and rivers together with fluvial incision would have led to the exposure of lake and fluvial sediments. The dry lake/river beds and other parts of exposed alluvial plains would have become dust sources for the *Xiashu* loess. It is reasonable to expect that the desert-like region would have expanded since the loose material would have been readily deflated and redeposited during the season of wind activity. This interpretation is supported by the view that deserts can form rapidly in response to increased aridity, together with the availability of a sufficient supply of sediment (Yang et al., 2011).

Our study has provided strong evidence that the alluvial plains in the northern subtropical region became an important dust source for southern China during Last glacial. The role of dust in climate change has become a major focus of Earth system modeling (e.g. Kohfeld and Harrison, 2001) and determining dust sources is an important objective of research on past dust cycles. The intensified aridification in northern subtropical China provides an important constraint on land surface conditions for future Earth system modelling which incorporates past dust cycles.

5. Conclusions

We have analyzed the major and trace element composition of samples from 22 *Xiashu* loess sections covering most of the loess region in the lower reaches of the Yangtze River valley and to the north of its lower reaches. To date, our dataset is the largest and most detailed for the region, with the most extensive spatial coverage. The geochemical composition of the *Xiashu* loess was compared with that of three potential dust sources: the sediments of the Yangtze River and the Yellow River, and the sediments of the deserts of the Asian interior (the average composition of which is inferred from the eolian deposits of the Chinese Loess Plateau). The results enable us to reach a definitive conclusion regarding the provenance of the *Xiashu* loess, and in addition they enable a comprehensive characterization of the provenance diversity of the loess in the region to the north of the Yangtze River, as well as for the loess in the Yangtze River valley. The main conclusions are as follows:

(1) The difference in the geochemical compositions of the <20 μm fraction between the *Xiashu* loess and the potential source materials indicates that neither the deserts in the Asian interior nor the floodplains of the Yangtze and the Yellow rivers are the primary provenance for the *Xiashu* loess in the region north of the Yangtze River.
(2) The results highlight the significant spatial heterogeneity of the geochemical composition of the *Xiashu* loess, which is in sharp contrast with the homogeneity of the loess of the Chinese Loess Plateau. This heterogeneity suggests a relatively short transport distance for the southern dust, and also that is comparatively poorly mixed.
(3) The floodplain of the Yangtze River supplied dust for the loess deposits downwind, while the floodplain of the Yellow River supplied some of the dust for the *Xiashu* loess deposits in a small area in the upper reaches of the Huai River. The alluvial plain in the present drainage of the Huai River was the primary dust source for the *Xiashu* loess in the main region between the Huai River and the Yangtze River; in addition, there are multiple local dust sources on the alluvial plain, as evidenced by the geochemical heterogeneity.
(4) Multiple local dust sources for the *Xiashu* loess in the present drainage of the Huai River indicate the occurrence of intensified aridity in northern subtropical China during the Last Glacial, highlighting the role of the glacial aridification of the present humid northern subtropical region for dust supply to the climate system.

Acknowledgments

This study was supported by the National Natural Science Foundation of China (projects 41625010, 41888101, 41430531 and 41690114), the Strategic Priority Research Program of Chinese Academy of Sciences (grant XDB26000000), and the National Key Research and Development Program (2017YFE0112800). We are grateful to the editor, Professor Xiaoping Yang, and two anonymous reviewers for the constructive comments and suggestions. We thank Dr. Jan Bloemendal for constructive discussions and English improvement.

Appendix A. Supplementary data

Supplementary data to this article can be found online at https://doi.org/10.1016/j.quascirev.2019.04.002.

References

Aleinikoff, J.N., Muhs, D.R., Bettis, E.A., Johnson, W.C., Fanning, C.M., Benton, R., 2008. Isotopic evidence for the diversity of late Quaternary loess in Nebraska: glaciogenic and nonglaciogenic sources. Geol. Soc. Am. Bull. 120, 1362–1377.

Assallay, A., Rogers, C., Smalley, I., Jefferson, I., 1998. Silt: 2–62 μm, 9–4φ. Earth Sci. Rev. 45, 61–88.
Bhatia, M.R., Crook, K.A., 1986. Trace element characteristics of graywackes and tectonic setting discrimination of sedimentary basins. Contrib. Mineral. Petrol. 92, 181–193.
Broecker, W.S., Peng, T.H., 1982. Tracers in the Sea. Eldigio Press, New York.
Brown, D.J., Helmke, P.A., Clayton, M.K., 2003. Robust geochemical indices for redox and weathering on a granitic laterite landscape in Central Uganda. Geochim. Cosmochim. Acta 67, 2711–2723.
Che, X.D., Li, G.J., 2013. Binary sources of loess on the Chinese Loess Plateau revealed by U–Pb ages of zircon. Quat. Res. 80, 545–551.
Chen, J., Li, G.J., Yang, J.D., Rao, W.B., Lu, H.Y., Balsam, W., Sun, Y.B., Ji, J.F., 2007. Nd and Sr isotopic characteristics of Chinese deserts: implications for the provenances of Asian dust. Geochim. Cosmochim. Acta 71, 3904–3914.
Chen, Z., Li, G.J., 2013. Evolving sources of eolian detritus on the Chinese Loess Plateau since early Miocene: tectonic and climatic controls. Earth Planet. Sci. Lett. 371–372, 220–225.
Condie, K.C., Dengate, J., Cullers, R.L., 1995. Behavior of rare earth elements in a paleoweathering profile on granodiorite in the Front Range, Colorado, USA. Geochim. Cosmochim. Acta 59, 279–294.
Condie, K.C., 2005. High field strength element ratios in Archean basalts: a window to evolving sources of mantle plumes? Lithos 79, 491–504.
Cullers, R.L., Basu, A., Suttner, L.J., 1988. Geochemical signature of provenance in sand-size material in soils and stream sediments near the Tobacco Root batholith, Montana, U.S.A. Chem. Geol. 70, 335–348.
Eby, G.N., 1990. The A-type granitoids: a review of their occurrence and chemical characteristics and speculations on their petrogenesis. Lithos 26, 115–134.
Fang, Q., Hong, H., Zhao, L., Furnes, H., Lu, H., Han, W., Liu, Y., Jia, Z., Wang, C., Yin, K., Algeo, T.J., 2017. Tectonic uplift-influenced monsoonal changes promoted hominin occupation of the Luonan Basin: insights from a loess-paleosol sequence, eastern Qinling Mountains, central China. Quat. Sci. Rev. 169, 312–329.
Fedo, C.M., Nesbitt, H.W., Young, G.M., 1995. Unraveling the effects of potassium metasomatism in sedimentary rocks and paleosols, with implications for paleoweathering conditions and provenance. Geology 23, 921–924.
Gu, Z.Y., 1987. A preliminary study on quartz oxygen isotope in Chinese loess and soils. In: Liu, T.S., et al. (Eds.), Aspects of Loess Research. China Ocean Press, Beijing, pp. 291–301, 1987.
Gu, Z.Y., 1999. Weathering Histories of Chinese Dust Deposits Based on Uranium and Thorium Series Nuclides, Cosmogenic ^{10}Be, and Major Elements. Ph.D. Thesis. Institute of Geology and Goephysics, Chinese Academy of Sciences, Beijing, China (in Chinese, with English Abstract).
Guan, H.C., Zhu, C., Zhu, T.X., Wu, L., Li, Y.H., 2016. Grain size, magnetic susceptibility and geochemical characteristics of the loess in the Chaohu lake basin: implications for the origin, palaeoclimatic change and provenance. J. Asian Earth Sci. 117, 170–183.
Guo, Z.T., Biscaye, P., Wei, L.Y., Chen, X.H., Peng, S.Z., Liu, T.S., 2000. Summer monsoon variations over the last 1.2 Ma from the weathering of loess-soil sequences in China. Geophys. Res. Lett. 27, 1751–1754.
Guo, Z.T., Peng, S.Z., Hao, Q.Z., Biscaye, P.E., Liu, T.S., 2001. Origin of the Miocene–Pliocene red-earth formation at Xifeng in northern China and implications for paleoenvironments. Palaeogeogr. Palaeoclimatol. Palaeoecol. 170, 11–26.
Guo, Z.T., Ruddiman, W.F., Hao, Q.Z., Wu, H.B., Qiao, Y.S., Zhu, R.X., Peng, S.Z., Wei, J.J., Yuan, B.Y., Liu, T.S., 2002. Onset of Asian desertification by 22 Myr ago inferred from loess deposits in China. Nature 416, 159–163.
Hao, Q.Z., Guo, Z.T., 2004. Magnetostratigraphy of a late Miocene-Pliocene loess-soil sequence in the western Loess Plateau in China. Geophys. Res. Lett. 31, L09209. https://doi:10.1029/2003GL019392.
Hao, Q.Z., Guo, Z.T., 2005. Spatial variations of magnetic susceptibility of Chinese loess for the last 600 kyr: implications for monsoon evolution. J. Geophys. Res. 110, B12101. https://doi: 10.1029/2005JB003765.
Hao, Q.Z., Guo, Z.T., Qiao, Y.S., Xu, B., Oldfield, F., 2010. Geochemical evidence for the provenance of middle Pleistocene loess deposits in southern China. Quat. Sci. Rev. 29, 3317–3326.
Hao, Q.Z., Wang, L., Oldfield, F., Peng, S.Z., Qin, L., Song, Y., Xu, B., Qiao, Y.S., Bloemendal, J., Guo, Z.T., 2012. Delayed build-up of Arctic ice sheets during 400,000-year minima in insolation variability. Nature 490, 393–396.
Hong, H.L., Gu, Y.S., Li, R.B., Zhang, K.X., Li, Z.H., 2009. Clay mineralogy and geochemistry and their palaeoclimatic interpretation of the Pleistocene deposits in the Xuancheng section, southern China. J. Quat. Sci. 25, 662–674.
Hong, H.L., Wang, C.W., Zeng, K.F., Gu, Y.S., Wu, Y.B., Yin, K., Li, Z.H., 2013. Geochemical constraints on provenance of the mid-Pleistocene red earth sediments in subtropical China. Sediment. Geol. 290, 97–108.
Hu, F.G., Yang, X.P., 2016. Geochemical and geomorphological evidence for the provenance of aeolian deposits in the Badain Jaran Desert, northwestern China. Quat. Sci. Rev. 131, 179–192.
Jahn, B.M., Gallet, S., Han, J.M., 2001. Geochemistry of the Xining, Xifeng and Jixian sections, Loess Plateau of China: eolian dust provenance and paleosol evolution during the last 140 ka. Chem. Geol. 178, 71–94.
Kahmann, J.A., Seaman III, J., Driese III, S.G., 2008. Evaluating trace elements as paleoclimate indicators: multivariate statistical analysis of late Mississippian Pennington Formation paleosols, Kentucky, USA. J. Geol. 116, 254–268.
Kemp, A., Thomas, R., Dell, C., Jaquet, J.-M., 1976. Cultural impact on the geochemistry of sediments in Lake Erie. J. Fish. Res. Board Can. 33, 440–462.
Kohfeld, K.E., Harrison, S.P., 2001. DIRTMAP: the geological record of dust. Earth Sci. Rev. 54, 81–114.
Kurtz, A.C., Derry, L.A., Chadwick, O.A., Alfano, M.J., 2000. Refractory element mobility in volcanic soils. Geology 28, 683–686.
Lai, Z.P., Zhang, W.G., Chen, X., Jia, Y.L., Liu, X.J., Fan, Q.S., Long, H., 2010. OSL chronology of loess deposits in East China and its implications for East Asian monsoon history. Quat. Geochronol. 5, 154–158.
Li, C.X., Wang, P., Sun, H.P., Zhang, J.Q., Fan, D.D., Deng, B., 2002. Late Quaternary incised-valley fill of the Yangtze delta (China): its stratigraphic framework and evolution. Sediment. Geol. 152, 133–158.
Li, G.J., Chen, J., Ji, J.F., Yang, J.D., Conway, T.M., 2009a. Natural and anthropogenic sources of East Asian dust. Geology 37, 727–730.
Li, G.J., L, L., Xu, S.J., Li, X.S., Chen, J., 2017a. Dust source of the loess deposits in the Eastern China constrained by uranium comminution age. Quat. Sci. 37, 1037–1044 (in Chinese, with English Abstract).
Li, L., Chen, J., Chen, Y., Hedding, D.W., Li, T., Li, L.F., Liu, X.J., Zeng, F.M., Wu, W.H., Zhao, L., Li, G.J., 2018. Uranium isotopic constraints on the provenance of dust on the Chinese Loess Plateau. Geology 46, 747–750.
Li, N., Hao, Q.Z., Zhang, X.J., Gao, X.B., Han, L., Zhang, W., Peng, S.Z., Wang, L., Xu, B., Qiao, Y.S., 2016. Geochemical evidence for the provenance of loess deposits in the Eastern Qinling Mountains, central China. Quat. Sci. 36, 332–346 (in Chinese, with English Abstract).
Li, X.S., Yang, D.Y., Lu, H.Y., 2001. Grain-size features and genesis of the Xiashu loess in Zhenjiang. Mar. Geol. Quat. Geol. 21, 25–32 (in Chinese, with English Abstract).
Li, X.S., Han, Z.Y., Yang, D.Y., Chen, Y.Y., 2006. REE geochemistry of Xiashu loess in Zhenjiang, Jiangsu Province. Acta Pedol. Sin. 43, 1–7 (in Chinese, with English Abstract).
Li, X.S., Han, Z.Y., Chen, Y., Cai, Y.F., Yang, D.Y., 2009b. Characteristics and source of raindust in Nanjing on March 11,2006. Quat. Sci. 29, 43–55 (in Chinese, with English Abstract).
Li, X.S., Han, Z.Y., Lu, H.Y., Chen, Y.Y., Li, Y., Yuan, X.K., Zhou, Y.W., Jiang, M.Y., Lv, C.J., 2017b. Onset of Xiashu loess deposition in southern China by 0.9 Ma and its implications for regional aridification. Sci. China Earth Sci. 3, 1–14.
Li, Y.R., Li, J., Zhu, S., 1935. The geology of Ningzhen mountain. Acta Geol. Acad. Sin. 11, 1–387 (in Chinese).
Liu, C.Q., Masuda, A., Okada, A., Yabuki, S., Fan, Z.L., 1994. Isotope geochemistry of Quaternary deposits from the arid lands in northern China. Earth Planet. Sci. Lett. 127, 25–38.
Liu, F., Li, G.J., Chen, J., 2014. U-Pb ages of zircon grains reveal a proximal dust source of the Xiashu loess, lower Yangtze River region, China. Chin. Sci. Bull. 59, 2391–2395.
Liu, J., W, X.H., Li, S.Q., Z, M.S., 1997. The last glacial stratigraphic sequence, depositional environment and climatic fluctuations from the aeolian sand dune in Hongguang, Pengze, Jiangxi (China). Quat. Sci. Rev. 16, 535–546.
Liu, Q.Q., Yang, X.P., 2018. Geochemical composition and provenance of aeolian sands in the Ordos Deserts, northern China. Geomorphology 318, 354–374.
Liu, T.S., 1985. Loess and the Environment. China Ocean Press, Beijing.
Liu, Z.T., Yang, X.P., 2013. Geochemical-geomorphological evidence for the provenance of aeolian sands and sedimentary environments in the Hunshandake Sandy Land, eastern Inner Mongolia, China. Acta. Geol. Sin-Engl. 87, 871–884.
Loring, D.H., 1991. Normalization of heavy-metal data from estuarine and coastal sediments. ICES J. Mar. Sci. 48, 101–115.
Marques, J.J., Schulze, D.G., Curi, N., Mertzman, S.A., 2004. Trace element geochemistry in Brazilian Cerrado soils. Geoderma 121, 31–43.
Muhs, D.R., Bettis, E.A., 2000. Geochemical variations in Peoria Loess of western Iowa indicate paleowinds of midcontinental North America during last glaciation. Quat. Res. 53, 49–61.
Muhs, D.R., Budahn, J.R., 2006. Geochemical evidence for the origin of late Quaternary loess in central Alaska. Can. J. Earth Sci. 43, 323–337.
Muhs, D.R., Budahn, J.R., Prospero, J.M., Carey, S.N., 2007. Geochemical evidence for African dust inputs to soils of western Atlantic islands: Barbados, the Bahamas, and Florida. J. Geophys. Res.-Earth 112, F02009. https://doi:10.1029/2005JF000445.
Nesbitt, H.W., 1979. Mobility and fractionation of rare earth elements during weathering of a granodiorite. Nature 279, 206–210.
Nesbitt, H.W., Young, G.M., 1984. Prediction of Some weathering trends of plutonic and volcanic rocks based on thermodynamic and kinetic considerations. Geochim. Cosmochim. Acta 48, 1523–1534.
Nesbitt, H., Muir, I., 1988. SIMS depth profiles of weathered plagioclase and processes affecting dissolved Al and Si in some acidic soil solutions. Nature 334, 336–338.
Nesbitt, H.W., Wilson, R.E., 1992. Recent chemical weathering of basalts. Am. J. Sci. 292, 740–777.
Peng, S.Z., Guo, Z.T., 2001. Geochemical indicator of original eolian grain size and implications on winter monsoon evolution. Sci. in China Ser. D. 44, 261–266.
Peng, S.Z., Hao, Q.Z., Wang, L., Ding, M., Zhang, W., Wang, Y.N., Guo, Z.T., 2016. Geochemical and grain-size evidence for the provenance of loess deposits in the Central Shandong Mountains region, northern China. Quat. Res. 85, 290–298.
Porter, S.C., 2001. Chinese loess record of monsoon climate during the last glacial–interglacial cycle. Earth Sci. Rev. 54, 115–128.
Prins, M.A., Zheng, H., Beets, K., Troelstra, S., Bacon, P., Kamerling, I., Wester, W., Konert, M., 2009. Dust supply from river floodplains: the case of the lower Huang He (Yellow River) recorded in a loess–palaeosol sequence from the

Mangshan Plateau. J. Quat. Sci. 24, 75–84.
Pullen, A., Kapp, P., McCallister, A.T., Chang, H., Gehrels, G.E., Garzione, C.N., Heermance, R.V., Ding, L., 2011. Qaidam Basin and northern Tibetan Plateau as dust sources for the Chinese Loess Plateau and paleoclimatic implications. Geology 39, 1031–1034.
Pye, K., 1995. The nature, origin and accumulation of loess. Quat. Sci. Rev. 14, 653–667.
Qian, P., Zheng, X.M., Cheng, J., Han, Y.J., Dong, Y., Zhang, J.G., 2018. Tracing the provenance of aeolian loess in the Yangtze River Delta through zircon U–Pb age and geochemical investigations. J. Mt. Sci. 15, 708–721.
Qiao, Y.S., Guo, Z.T., Hao, Q.Z., Wu, W.X., Jiang, W.Y., Yuan, B.Y., Zhang, Z.S., Wei, J.J., Zhao, H., 2003. Loess-soil sequences in southern Anhui Province: magneto-stratigraphy and paleoclimatic significance. Chin. Sci. Bull. 48, 2088–2093.
Qiao, Y.S., Hao, Q.Z., Peng, S.S., Wang, Y., Li, J.W., Liu, Z.X., 2011. Geochemical characteristics of the eolian deposits in southern China, and their implications for provenance and weathering intensity. Palaeogeogr. Palaeoclimatol. Palaeoecol. 308, 513–523.
Ren, X.Z., Yang, X.P., Wang, Z.T., Zhu, B.Q., Zhang, D.G., Rioual, P., 2014. Geochemical evidence of the sources of aeolian sands and their transport pathways in the Minqin Oasis, northwestern China. Quat. Int. 334–335, 165–178.
Rohling, E.J., Fenton, M., Jorissen, F.J., Bertrand, P., Ganssen, G.M., Caulet, J.P., 1998. Glacial sea level lowstands of the last 500,000 years. Nature 394, 162–165.
Rohling, E.J., Grant, K., Bolshaw, M., Roberts, A.P., Siddall, M., Hemleben, C., Kucera, M., 2009. Antarctic temperature and global sea level closely coupled over the past five glacial cycles. Nat. Geosci. 2, 500–504.
Shang, Y., Prins, M.A., Beets, C.J., Kaakinen, A., Lahaye, Y., Dijkstra, N., Rits, D.S., Wang, B., Zheng, H.B., van Balen, R.T., 2018. Aeolian dust supply from the Yellow River floodplain to the Pleistocene loess deposits of the Mangshan Plateau, central China: evidence from zircon U-Pb age spectra. Quat. Sci. Rev. 182, 131–143.
Shao, J.J., 1988. The origin of the Xiashu loess in the lower reaches of the Yangtze River. Reg. Geol. China 4, 24–31 (in Chinese, with English Abstract).
Shao, Y., Dong, C.H., 2006. A review on East Asian dust storm climate, modelling and monitoring. Glob. Planet. Chang. 52, 1–22.
Sheldon, N.D., Tabor, N.J., 2009. Quantitative paleoenvironmental and paleoclimatic reconstruction using paleosols. Earth Sci. Rev. 95, 1–52.
Smalley, I., O'Hara-Dhand, K., Wint, J., Machalett, B., Jary, Z., Jefferson, I., 2009. Rivers and loess: the significance of long river transportation in the complex event-sequence approach to loess deposit formation. Quat. Int. 198, 7–18.
Smith, J., Vance, D., Kemp, R.A., Archer, C., Toms, P., King, M., Zárate, M., 2003. Isotopic constraints on the source of Argentinian loess–with implications for atmospheric circulation and the provenance of Antarctic dust during recent glacial maxima. Earth Planet. Sci. Lett. 212, 181–196.
Sugitani, K., Horiuchi, Y., Adachi, M., Sugisaki, R., 1996. Anomalously low Al_2O_3/TiO_2 values for Archean cherts from the Pilbara Block, Western Australia—possible evidence for extensive chemical weathering on the early earth. Precambr. Res. 80, 49–76.
Sun, J.M., Zhang, M.Y., Liu, T.S., 2001. Spatial and temporal characteristics of dust storms in China and its surrounding regions, 1960–1999: relations to source area and climate. J. Geophys. Res. 106, 10325–10333.
Sun, J.M., 2002. Provenance of loess material and formation of loess deposits on the Chinese Loess Plateau. Earth Planet. Sci. Lett. 203, 845–859.
Sun, J.M., Ye, J., Wu, W.Y., Ni, X.J., Bi, S.D., Zhang, Z.Q., Liu, W.M., Meng, J., 2010. Late Oligocene–Miocene mid-latitude aridification and wind patterns in the Asian interior. Geology 38, 515–518.
Tan, S.C., Li, J.W., Che, H.Z., Chen, B., Wang, H., 2017. Transport of East Asian dust storms to the marginal seas of China and the southern North Pacific in spring 2010. Atmos. Environ. 148, 316–328.
Taylor, S.R., Mclennan, S.M., Mcculloch, M.T., 1983. Geochemistry of loess, continental crustal composition and crustal model ages. Geochim. Cosmochim. Acta 47, 1897–1905.
Taylor, S.R., McLennan, S.M., 1985. The Continental Crust: its Composition and Evolution. Blackwell, Oxford.
Tsoar, H., Pye, K., 1987. Dust transport and the question of desert loess formation. Sedimentology 34, 139–153.
Uno, I., Satake, S., Carmichael, G.R., Tang, Y.H., Wang, Z.F., Takemura, T., Sugimoto, N., Shimizu, A., Murayama, T., Cahill, T.A., Cliff, S., Uematsu, M., Ohta, S., Quinn, P.K., Bates, T.S., 2004. Numerical study of Asian dust transport during the springtime of 2001 simulated with the Chemical Weather Forecasting System (CFORS) model. J. Geophys. Res. 109, D19S24. https://doi:10.1029/2003JD004222.
Wang, L., Jiang, W.Y., Jiang, D.B., Zou, Y.F., Liu, Y.Y., Zhang, E.L., Hao, Q.Z., Zhang, D.G., Zhang, D.T., Peng, Z.Y., Xu, B., Yang, X.D., Lu, H.Y., 2018. Prolonged heavy snowfall during the Younger Dryas. J. Geophys. Res. 123, 13748–13762.
Wang, P.X., 1999. Response of Western Pacific marginal seas to glacial cycles: paleoceanographic and sedimentological features. Mar. Geol. 156, 5–39.
Wang, X.Y., Lu, H.Y., Zhang, H.Z., Wu, J., Hou, X.X., Fu, Y., Geng, J.Y., 2017. Distribution, provenance, and onset of the Xiashu Loess in Southeast China with paleoclimatic implications. J. Asian Earth Sci. 155, 180–187.
Winchester, J.A., Floyd, P.A., 1977. Geochemical discrimination of different magma series and their differentiation products using immobile elements. Chem. Geol. 20, 325–343.
Wu, J., Fu, C.B., Jiang, W.M., Liu, H.N., Zhao, R.H., 2005. Preliminary simulation research of direct radiative forcing of mineral dust aerosol over east Asia region. Chin. J. Geophys. 48, 1336–1347.
Xia, Y.F., Wang, Y.J., 1999. An important stratigraphic boundary in dust accumulation, South China: evidence from magnetic susceptibility. Chin. Sci. Bull. 44, 189–192.
Xu, Y.Z., 1991. Preliminary study on the time and forming of the Xiashu loess, Hefei. Anhui Geol. 1, 54–66 (in Chinese, with English Abstract).
Yang, D.Y., 1986. The paleoenvironment of the mid-lower regions of Changjiang in the full-glacial period of late Pleistocene. Acta Geog. Sin. 4, 302–310 (in Chinese, with English Abstract).
Yang, D.Y., 1991. The Quaternary dust-fall accumulation and the monsoon variability in eastern China. Quat. Sci. 4, 354–360 (in Chinese, with English Abstract).
Yang, S.Y., Li, C.X., Yang, D.Y., Li, X.S., 2004. Chemical weathering of the loess deposits in the lower Changjiang Valley, China, and paleoclimatic implications. Quat. Int. 117, 27–34.
Yi, S.W., Li, X.S., Han, Z.Y., Lu, H.Y., Liu, J.F., Wu, J., 2018. High resolution luminescence chronology for Xiashu Loess deposits of Southeastern China. J. Asian Earth Sci. 155, 188–197.
Yang, X.P., Liu, Y.S., Li, C.Z., Song, Y.L., Zhu, H.P., Jin, X.D., 2007a. Rare earth elements of aeolian deposits in Northern China and their implications for determining the provenance of dust storms in Beijing. Geomorphology 87, 365–377.
Yang, X.P., Zhu, B.Q., White, P.D., 2007b. Provenance of aeolian sediment in the Taklamakan Desert of western China, inferred from REE and major-elemental data. Quat. Int. 175, 71–85.
Yang, X.P., Zhang, F., Fu, X.D., Wang, X.M., 2008. Oxygen isotopic compositions of quartz in the sand seas and sandy lands of northern China and their implications for understanding the provenances of aeolian sands. Geomorphology 102, 278–285.
Yang, X.P., Scuderi, L., Paillou, P., Liu, Z.T., Li, H.W., Ren, X.Z., 2011. Quaternary environmental changes in the drylands of China – a critical review. Quat. Sci. Rev. 30, 3219–3233.
Yu, H.J., 1999. A new exploration on the origin of loess in the shelf area of the eastern China seas. Quat. Sci. 7, 367–372 (in Chinese, with English Abstract).
Zhang, H., Song, C.Z., 2013. Geochemical characteristics of loess-palaeosols from the northern slope of Dabie Mountain and research of its provenance in the enrichment factor way. Geol. Sci.Tech. Inf. 3, 87–93 (in Chinese, with English Abstract).
Zhang, H.Y., Lu, H.Y., Jiang, S.Y., Vandenberghe, J., Wang, S.J., Cosgrove, R., 2012. Provenance of loess deposits in the Eastern Qinling Mountains (central China) and their implications for the paleoenvironment. Quat. Sci. Rev. 43, 94–102.
Zhang, W.G., Yu, L.Z., Lu, M., Zheng, X.M., Shi, Y.X., 2007. Magnetic properties and geochemistry of the Xiashu Loess in the present subtropical area of China, and their implications for pedogenic intensity. Earth Planet. Sci. Lett. 260, 86–97.
Zhang, Y., Sperber, K.R., Boyle, J.S., 1997. Climatology and interannual variation of the East Asian winter monsoon: results from the 1979–95 NCEP/NCAR reanalysis. Mon. Weather Rev. 125, 2605–2619.
Zhao, S.L., Li, G.G., 1990. Desertization on the shelves adjacent China in the later Pleistocene. Chin. J. Oceanol. Limnol. 8, 289–298.
Zhao, T.L., Gong, S.L., Zhang, X.Y., McKendry, I.G., 2003. Modeled size-segregated wet and dry deposition budgets of soil dust aerosol during ACE-Asia 2001: implications for trans-Pacific transport. J. Geophys. Res. 108 (D23), 8665. https://doi.org/10.1029/2002JD003363.
Zheng, H.B., Huang, X.T., Ji, J.L., Liu, R., Zeng, Q.Y., Jiang, F.C., 2007. Ultra-high rates of loess sedimentation at Zhengzhou since stage 7: implication for the Yellow river erosion of the Sanmen gorge. Geomorphology 85, 131–142.
Zhu, Y., Chang, R., 2000. Preliminary study of the dynamic origin of the distribution pattern of bottom sediments on the continental shelves of the Bohai Sea, Yellow Sea and East China Sea. Estuar. Coast. Shelf Sci. 51, 663–680.